

Evolution of the modern  
human brain pp. 124 & 165

Rapid injection molding  
of glass pp. 126 & 182

Urgent actions to redress  
inequities in science p. 133

# Science

\$15  
9 APRIL 2021  
sciencemag.org

AAAS

## MAGNETARS

How hypermagnetized neutron stars power  
cosmic explosions p. 120

# Aims and scope

*Science* is a leading outlet for scientific news, commentary, and cutting-edge research. Through its print and online incarnations, *Science* reaches an estimated worldwide readership of more than one million. *Science*'s authorship is global too, and its articles consistently rank among the world's most cited research.

*Science* serves as a forum for discussion of important issues related to the advancement of science by publishing material on which a consensus has been reached as well as including the presentation of minority or conflicting points of view. Accordingly, all articles published in *Science*—including editorials, news and comment, and book reviews—are signed and reflect the individual views of the authors and not official points of view adopted by AAAS or the institutions with which the authors are affiliated.

# Editorial Board

## Science Research and Insights Editors

To learn more about the backgrounds and areas of emphasis of the editors below, and for contact information, see our [Meet the Editors](#) page.

**Deputy Editor, Cambridge** Stella M. Hurtley (UK)

**Deputy Editor, Insights** Gemma Alderton (UK)

**Deputy Editors, Research** Phillip D. Szuromi, Sacha Vignieri

**Senior Editors** Caroline Ash (UK), Michael A. Funk, Brent Grocholski, Di Jiang, Priscilla N. Kelly, Marc S. Lavine (Canada), Mattia Maroso, Yevgeniya Nusinovich, Ian S. Osborne (UK), L. Bryan Ray, Seth Thomas Scanlon (UK), H. Jesse Smith, Keith T. Smith (UK), Jelena Stajic, Peter Stern (UK), Valerie B. Thompson, Brad Wible

**Associate Editors** Bianca Lopez, Madeleine Seale (UK), Corinne Simonti, Yury V. Suleymanov, Ekeoma Uzogara

**Letters Editor** Jennifer Sills

**Lead Content Production Editors** Chris Filiatreau, Harry Jach

**Senior Content Production Editor** Amelia Beyna

**Content Production Editors** Robert French, Julia Haber-Katris, Nida Masiulis, Abigail Shashikanth, Suzanne M. White

**Senior Editorial Managers** Carolyn Kyle, Beverly Shields

**Senior Program Associate** Maryrose Madrid

**Editorial Associate** Joi S. Granger

**Senior Editorial Coordinators** Aneera Dobbins, Jeffrey Hearn, Lisa Johnson, Jerry Richardson, Alice Whaley (UK), Anita Wynn

**Editorial Coordinators** Maura Byrne, Clair Goodhead (UK), Alexander Kief, Ronmel Navas, Isabel Schnaidt, Qiyam Stewart, Brian White

**Research and Data Analyst** Jessica L. Slater

**Administrative Coordinator** Karalee P. Rogers

**ASI Director, Operations** Janet Clements (UK)

**ASI Senior Office Administrator** Jessica Waldock (UK)

## Board of Reviewing Editors

**Erin Adams**

University of Chicago

**Takuzo Aida**

University of Tokyo

**Leslie Aiello**

Wenner-Gren Foundation

**Deji Akinwande**

University of Texas at Austin

**Judith Allen**

University of Manchester

**James Analytis**

University of California, Berkeley

**Paola Arlotta**

Harvard University

**Delia Baldassarri**

New York University

**Nenad Ban**

ETH Zürich

**Christopher Barratt**

University of Dundee

**Nandita Basu**

University of Waterloo

**Franz Bauer**

Pontificia Universidad Católica de Chile

**Ray H. Baughman**

University of Texas at Dallas

**Carlo Beenakker**

Leiden University

**Yasmine Belkaid**

National Institute of Allergy and Infectious Diseases, National Institutes of Health

**Philip Benfey**

Duke University

**Kiros T. Berhane**

Columbia University

**Joseph J. Berry**

National Renewable Energy Laboratory

**Alessandra Biffi**

Harvard Medical School

**Chris Bowler**

École Normale Supérieure

**Ian Boyd**

University of St. Andrews

**Malcolm Brenner**

Baylor College of Medicine

**Emily Brodsky**

University of California, Santa Cruz

**Christian Büchel**

Universitätsklinikum Hamburg-Eppendorf

**Johannes Buchner**

Technische Universität München

**Dennis R. Burton**

Scripps Research

**Carter Tribble Butts**

University of California, Irvine

**György Buzsáki**

New York University School of Medicine

**Mariana Byndloss**

Vanderbilt University Medical Center

**Anmarie Carlton**

University of California, Irvine

**Simon Cauchemez**

Institut Pasteur

**Ling-Ling Chen**

Shanghai Institute of Biochemistry and Cell Biology, Chinese Academy of Sciences

**Wendy Cho**

University of Illinois Urbana-Champaign

**Ib Chorkendorff**

Technical University of Denmark

**Chunaram Choudhary**

Københavns Universitet

**Karlene Cimprich**

Stanford University

**Laura Colgin**

University of Texas at Austin

**James J. Collins**

Massachusetts Institute of Technology

**Robert Cook-Deegan**

Arizona State University

**Virginia Cornish**

Columbia University

**Carolyn Coyne**

Duke University

**Roberta Croce**

Vrije Universiteit Amsterdam

**Christina Curtis**

Stanford University

**Molly Crocket**

Princeton University

**Ismaila Dabo**

Pennsylvania State University

**Jeff L. Dangl**

University of North Carolina at Chapel Hill

**Nicolas Dauphas**

University of Chicago

**Frans de Waal**

Emory University

**Claude Desplan**

New York University

**Sandra Díaz**

Universidad Nacional de Córdoba

**Samuel Díaz-Muñoz**

University of California, Davis

**Ulrike Diebold**

Technische Universität Wien

**Stefanie Dimmeler**

Goethe-Universität Frankfurt

**Hong Ding**

Institute of Physics, Chinese Academy of Sciences

**Dennis Discher**

University of Pennsylvania

**Jennifer A. Doudna**

University of California, Berkeley

**Ruth Drdla-Schutting**

Medical University of Vienna

**Raissa M. D'Souza**

University of California, Davis

**Bruce Dunn**

University of California, Los Angeles

**William Dunphy**

California Institute of Technology

**Scott Edwards**

Harvard University

**Todd Ehlers**

University of Tübingen

**Nader Engheta**

University of Pennsylvania

**Karen Ersche**

University of Cambridge

**Beate Escher**

Helmholtz Centre for Environmental Research – UFZ and University of Tübingen

**Barry Everitt**

University of Cambridge

**Vanessa Ezenwa**

University of Georgia

**Toren Finkel**

University of Pittsburgh Medical Center

**Gwenn Flowers**

Simon Fraser University

**Natascha Förster Schreiber**

Max Planck Institute for Extraterrestrial Physics, Garching

**Peter Fratzl**

Max Planck Institute of Colloids and Interfaces, Potsdam

**Elaine Fuchs**

Rockefeller University

**Caixia Gao**

Institute of Genetics and Developmental Biology, Chinese Academy of Sciences

**Daniel Geschwind**

University of California, Los Angeles

**Lindsey Gillson**

University of Cape Town

**Gillian Griffiths**

University of Cambridge

**Nicolas Gruber**

ETH Zürich

**Hua Guo**

University of New Mexico

**Taekjip Ha**

Johns Hopkins University

**Daniel Haber**

Massachusetts General Hospital

**Sharon Hammes-Schiffer**

Yale University

**Wolf-Dietrich Hardt**

ETH Zürich

**Louise Harra**

University College London

**Carl-Philipp Heisenberg**

Institute of Science and Technology Austria

**Janet G. Hering**

Swiss Federal Institute of Aquatic Science and Technology (Eawag)

**Christoph Hess**

University of Basel and University of Cambridge

**Heather Hickman**

National Institute of Allergy and Infectious Diseases, National Institutes of Health

**Hans Hilgenkamp**

University of Twente

**Janneke Hille Ris Lambers**

ETH Zürich

**Kai-Uwe Hinrichs**

University of Bremen

**Deirdre Hollingsworth**

University of Oxford

**Randall Hulet**

Rice University

**Auke Ijspeert**

École Polytechnique Fédérale in Lausanne

**Gwyneth Ingram**

École Normale Supérieure de Lyon

**Darrell Irvine**

Massachusetts Institute of Technology

**Akiko Iwasaki**

Yale University

**Erich Jarvis**

Rockefeller University

**Peter Jonas**

Institute of Science and Technology Austria

**Johanna Joyce**

Université de Lausanne

**Matt Kaeberlein**

University of Washington

**William Kaelin Jr.**

Dana-Farber Cancer Institute

**Daniel Kammen**

University of California, Berkeley

**Kisuk Kang**

Seoul National University

**V. Narry Kim**

Seoul National University

**Nancy Knowlton**

Smithsonian Institution

**Etienne Koechlin**

École Normale Supérieure

**Alex L. Kolodkin**

Johns Hopkins University

**LaShanda Korley**

University of Delaware

**Paul Kubes**

University of Calgary

**Chris Kuzawa**

Northwestern University

**Laura Lackner**

Northwestern University

**Mitchell A. Lazar**

University of Pennsylvania

**Hedwig Lee**

Duke University

**Ryan Lively**

Georgia Institute of Technology

**Luis Liz-Marzán**

CIC biomaGUNE

**Omar Lizardo**

University of California, Los Angeles

**Jonathan Losos**

Washington University in St. Louis

**Ke Lu**

Institute of Metal Research, Chinese Academy of Sciences

**Christian Lüscher**

University of Geneva

**Jean Lynch-Stieglitz**

Georgia Institute of Technology

**David Lyons**

University of Edinburgh

**Fabienne Mackay**

QIMR Berghofer Medical Research Institute

**Zeynep Madak-Erdogan**

University of Illinois Urbana-Champaign

**Vidya Madhavan**

University of Illinois Urbana-Champaign

**Anne Magurran**

University of St. Andrews

**Ari Pekka Mähönen**

University of Helsinki

**Asifa Majid**

University of Oxford

**Oscar Marín**

King's College London

**Charles Marshall**

University of California, Berkeley

**Christopher Marx**

University of Idaho

**David Masopust**

University of Minnesota

**Geraldine Masson**

Institut de Chimie des Substances Naturelles, CNRS

**Rodrigo Medellín**

Universidad Nacional Autónoma de México

**C. Jessica Metcalf**

Princeton University

**Tom Misteli**

National Cancer Institute, National Institutes of Health

**Daniel Neumark**

University of California, Berkeley

**Thi Hoang Duong Nguyen**

MRC Laboratory of Molecular Biology

**Beatriz Noheda**

University of Groningen

**Helga Nowotny**

Vienna Science, Research and Technology Fund

**Pilar Ossorio**

University of Wisconsin

**Andrew Oswald**

University of Warwick

**Isabella Pagano**

Istituto Nazionale di Astrofisica

**Jane Parker**

Max Planck Institute of Plant Breeding Research, Cologne

**Daniel Pauly**

University of British Columbia

**Ana Pêgo**

Universidade do Porto

**Samuel Pfaff**

Salk Institute for Biological Studies

**Julie Pfeiffer**

University of Texas Southwestern Medical Center at Dallas

**Philip Phillips**

University of Illinois Urbana-Champaign

**Mathieu Piel**

Institut Curie

**Kathrin Plath**

University of California, Los Angeles

**Martin Plenio**

Ulm University

**Katherine Pollard**

University of California, San Francisco

**Elvira Poloczanska**

Alfred-Wegener-Institut

**Julia Pongratz**

Ludwig Maximilians Universität

**Philippe Poulin**

Centre de Recherche Paul Pascal, CNRS

**Lei Stanley Qi**

Stanford University

**Trevor Robbins**

University of Cambridge

**Joeri Rogelj**

Imperial College London

**Amy Rosenzweig**

Northwestern University

**John Rubinstein**

The Hospital for Sick Children, University of Toronto

**Mike Ryan**

University of Texas at Austin

**Miquel Salmeron**

Lawrence Berkeley National Laboratory

**Nitin Samarth**

Pennsylvania State University

**Erica Ollmann Saphire**

La Jolla Institute for Immunology

**Joachim Saur**

Universität zu Köln

**Alexander Schier**

Harvard University

**Wolfram Schlenker**

Columbia University

**Susannah Scott**

University of California, Santa Barbara

**Anuj Shah**

University of Chicago

**Vladimir Shalaev**

Purdue University

**Jie Shan**

Cornell University



**Beth Shapiro**  
University of California, Santa Cruz

**Jay Shendure**  
University of Washington

**Steve Sherwood**  
University of New South Wales

**Brian Shoichet**  
University of California, San Francisco

**Robert Siliciano**  
Johns Hopkins University School of Medicine

**Lucia Sivilotti**  
University College London

**John Speakman**  
University of Aberdeen

**Allan C. Spradling**  
Carnegie Institution for Science

**V. S. Subrahmanian**  
Northwestern University

**Eriko Takano**  
University of Manchester

**A. Alec Talin**  
Sandia National Laboratories

**Patrick Tan**  
Duke-NUS Medical School

**Sarah Teichmann**  
Wellcome Sanger Institute

**Rocio Titiunik**  
Princeton University

**Shubha Tole**  
Tata Institute of Fundamental Research

**Maria-Elena Torres Padilla**  
Helmholtz Zentrum München

**Kimani Toussaint**  
Brown University

**Barbara Treutlein**  
ETH Zürich

**Jason Tylianakis**  
University of Canterbury

**Matthew Vander Heiden**  
Massachusetts Institute of Technology

**Wim van der Putten**  
Netherlands Institute of Ecology

**Ivo Vankelecom**  
Katholieke Universiteit Leuven

**Judith Varner**  
University of California, San Diego

**Henrique Veiga-Fernandes**  
Champalimaud Foundation

**Reinhilde Veugelers**  
Katholieke Universiteit Leuven

**Bert Vogelstein**  
Johns Hopkins University

**Julia Von Blume**  
Yale School of Medicine

**David Wallach**  
Weizmann Institute of Science

**Jessica Ware**  
American Museum of Natural History

**David Waxman**  
Fudan University

**Alex Webb**  
University of Cambridge

**Terrie Williams**  
University of California, Santa Cruz

**Hao Wu**  
Harvard University

**Li Wu**  
Tsinghua University

**Wei Xie**  
Tsinghua University

**Yu Xie**  
Princeton University

**Amir Yacoby**  
Harvard University

**Benjamin Youngblood**  
St. Jude Children's Research Hospital

**Jan Zaanen**  
Leiden University

**Kenneth Zaret**  
University of Pennsylvania School of Medicine

**Lidong Zhao**  
Beihang University

**Bing Zhu**  
Institute of Biophysics, Chinese Academy of Sciences

**Xiaowei Zhuang**  
Harvard University

**Maria Zuber**  
Massachusetts Institute of Technology

**Statistics Board of Reviewing Editors**

**Ron Brookmeyer**  
University of California, Los Angeles

**Gabriel Lander**  
Scripps Research

**Alison Motsinger-Reif**  
National Institute of Environmental Health Sciences, National Institutes of Health

**Giovanni Parmigiani**  
Dana-Faber Cancer Institute

**Richard Smith**  
University of North Carolina at Chapel Hill

**Jane-Ling Wang**  
University of California, Davis


**Chris Wikle**  
University of Missouri

**Ian A. Wilson**  
Scripps Research

## RESEARCH ARTICLES

### Imaging cell lineage with a synthetic digital recording system




BY KE-HUAN K. CHOW, MARK W. BUDDE, ALEJANDRO A. GRANADOS, MARIA CABRERA, SHINAE YOON, SOOMIN CHO, TING-HAO HUANG, NOUSHIN KOULENA, KIRSTEN L. FRIEDA, LONG CAI, [...] MICHAEL B. ELOWITZ **+1 authors** • 09 APR 2021 

A genetic editing system, intMEMOIR, reveals the lineage histories of individual cells within their native tissue context.

ABSTRACT 

### QSER1 protects DNA methylation valleys from de novo methylation



BY GARY DIXON, HENG PAN, DAPENG YANG, BESS P. ROSEN, THERANDE JASHARI, NIPUN VERMA, JULIAN PULECIO, INBAL CASPI, KIHYUN LEE, STEPHANIE STRANSKY, [...] DANWEI HUANGFU **+10 authors** • 09 APR 2021 

QSER1 cooperates with TET1 to safeguard DNA methylation valleys from DNMT3-mediated de novo methylation.

ABSTRACT 


#### RELATED

### The push and pull of DNA methylation

BY TIANPENG GU, MARGARET A. GOODELL

### Mechanism and dynamics of fatty acid photodecarboxylase



BY D. SORIGUÉ, K. HADJIDEMETRIOU, S. BLANGY, G. GOTTHARD, A. BONVALET, N. COQUELLE, P. SAMIRE, A. ALEKSANDROV, L. ANTONUCCI, A. BENACHIR, [...] F. BEISSON **+37 authors** • 09 APR 2021 

Snapshots of a photoenzyme reveal structural changes during fatty acid decarboxylation.

ABSTRACT 

## Bilateral visual projections exist in non-teleost bony fish and predate the emergence of tetrapods



BY ROBIN J. VIGOUROUX, KARINE DUROURE, JULIETTE VOUGNY, SHAHAD ALBADRI, PETER KOZULIN, ELOISA HERRERA, KIM NGUYEN-BA-CHARVET, INGO BRAASCH, RODRIGO SUÁREZ, FILIPPO DEL BENE, ALAIN CHÉDOTAL • 09 APR 2021 : 150-156

Bilateral vision preceded terrestrial life in evolutionary history.

ABSTRACT

## Targeting the nucleotide salvage factor DNPH1 sensitizes *BRCA*-deficient cells to PARP inhibitors



BY KASPER FUGGER, ILIRJANA BAJRAMI, MARIANA SILVA DOS SANTOS, SARAH JANE YOUNG, SIMONE KUNZELMANN, GEOFF KELLY, GRAEME HEWITT, HARSHIL PATEL, ROBERT GOLDSTONE, THOMAS CARELL, [...] STEPHEN C. WEST **+3 authors** • 09 APR 2021 : 156-165

Inhibiting DNPH1 provides a promising strategy for the hypersensitization of *BRCA*-deficient cancers to PARP inhibitor therapy.

ABSTRACT

### RELATED

#### Epigenetic nucleotides enhance therapy

BY SKIRMANTAS KRIAUCIONIS

## The primitive brain of early *Homo*



BY MARCIA S. PONCE DE LEÓN, THIBAUT BIENVENU, ASSAF MAROM, SILVANO ENGEL, PAUL TAFFOREAU, JOSÉ LUIS ALATORRE WARREN, DAVID LORDKIPANIDZE, IWAN KURNIAWAN, DELTA BAYU MURTI, RUSYAD ADI SURİYANTO, [...] CHRISTOPH P. E. ZOLLIKOFER **+1 authors** • 09 APR 2021 : 165-171

Early *Homo* evolved a modern humanlike brain organization only after its first dispersal from Africa.

ABSTRACT

### RELATED

#### The enigmatic origins of the human brain

BY AMÉLIE BEAUDET

# Pollen PCP-B peptides unlock a stigma peptide–receptor kinase gating mechanism for pollination



BY CHEN LIU, LIANPING SHEN, YU XIAO, DAVID VYSHEDSKY, CHAO PENG, XIANG SUN, ZHIWEN LIU, LIJUN CHENG, HUA ZHANG, ZHIFU HAN, [...] CHAO LI

+3 authors

• 09 APR 2021 : 171-175



Competing peptide signals regulate production of reactive oxygen species at the floral stigma to control response to pollen.

ABSTRACT ▾

---

## REVIEWS

### Epigenetics, fragmentomics, and topology of cell-free DNA in liquid biopsies



BY Y. M. DENNIS LO, DIANA S. C. HAN, PEIYONG JIANG, ROSSA W. K. CHIU • 09 APR 2021



ABSTRACT ▾

---

## TECHNICAL COMMENTS

### Comment on “Tumor-initiating cells establish an IL-33–TGF- $\beta$ niche signaling loop to promote cancer progression”



BY JASPER B. J. KAMPHUIS, WILLIAM P. M. WORRALL, JULIEN STACKOWICZ, AURÉLIE MOUGEL, EMILIE MAURÉ, EVA CONDE, PIERRE BRUHNS, LAURENT

GUILLEMINAULT, NICOLAS GAUDENZIO, JINMIAO CHEN, [...] LAURENT L. REBER

+1 authors

• 09 APR 2021



ABSTRACT ▾



## Supplementary Materials for **The primitive brain of early *Homo***

Marcia S. Ponce de León\*, Thibault Bienvenu, Assaf Marom, Silvano Engel, Paul Tafforeau, José Luis Alatorre Warren, David Lordkipanidze, Iwan Kurniawan, Delta Bayu Murti, Rusyad Adi Suriyanto, Toetik Koesbardiati, Christoph P. E. Zollikofer\*

\*Corresponding author. Email: [marcia@aim.uzh.ch](mailto:marcia@aim.uzh.ch) (M.S.P.d.L.); [zolli@aim.uzh.ch](mailto:zolli@aim.uzh.ch) (C.P.E.Z.)

Published 9 April 2021, *Science* **372**, 165 (2021)  
DOI: 10.1126/science.aaz0032

### **This PDF file includes:**

Materials and Methods  
Supplementary Text  
Figs. S1 to S5  
References

## Materials and Methods

### M1. Sample

The extant sample comprises crania of  $N_h=110$  modern humans (*Homo sapiens*),  $N_c=81$  chimpanzees (*Pan troglodytes* spp.),  $N_b=27$  bonobos (*Pan paniscus*),  $N_g=43$  gorillas (*Gorilla gorilla* spp.), and  $N_o=32$  orangutans (*Pongo pygmaeus*). Specimens were grouped according to their maxillary dental eruption stage (immature: one or more permanent molars fully erupted; adult: all permanent molars fully erupted). Specimens are from the Collections of the Department of Anthropology and Anthropological Museum of the University of Zurich, the Royal Museum for Central Africa (Tervuren), the Bavarian State Collection for Anthropology and Paleoanatomy (Munich), the Peabody Museum of Archaeology and Ethnology at Harvard University, the Natural History Museum London, and the Duckworth Collection at Cambridge University. The fossil sample consists of the specimens listed in Table 1 (see main text).

### M2. Computed Tomography and data segmentation

Computed Tomography (CT) of all specimens was performed with medical CT devices, using beam collimations between 0.5 and 1.0 mm, and performing cross-sectional image reconstructions with voxel sizes between  $0.2^3$  and  $0.5^3$  mm<sup>3</sup>. The Dmanisi cranium D4500 was further analyzed with synchrotron tomography on beamline ID17 at the European Synchrotron Radiation Facility (ESRF). The cranium was placed in a semolina-filled PVC cylinder to guarantee fixation and to prevent direct irradiation of the detector. Scanning parameters were as follows: 45 $\mu$ m taper optic with cerium-doped taper protection (required retrodistortion map application before further processing); energy: 96keV; propagation distance 5000mm; monochromator: Si 111 curved double Laue; sensor: FReLoN 2K14; camera mode: frame transfer mode, no shutter; scintillator: Gadox 60; insertion device: W150; ID Gap: 25mm; machine filling mode: 200mA; projection number: 5000; scan geometry: 360° in half-acquisition mode, step-by-step scanning; exposure time: 0.15s; time per scan: 37min; number of scans: 116; image reconstruction: single-distance retrieval using Paganin algorithm, ring artifact correction.

For each cranium, the endocranial surface was digitally extracted from the CT data volume following procedures described in ref. (87), and using the software packages Avizo and Geomagic Studio. Endocranial volumes (ECV) were evaluated from the surface data using the software Avizo.

### M3. Cranio-cerebral topographic criteria for the identification of frontal lobe structures on fossil endocasts

Broca's Cap (BC) is a conspicuous feature in the fronto-orbital region of both great ape and human endocasts, but the underlying brain areas are not homologous across groups (7, 8). In great apes, BC largely comprises Brodmann area 44, and its inferior delimitation is formed by the fronto-orbital sulcus (Fig. 1A, *fo*). In humans, BC largely comprises Brodmann areas 45 and 47, and its inferior delimitation tends to coincide with the lateral orbital sulcus (9) (Fig. 1B, *lo*). While the BC regions of great ape and human endocasts comprise different brain regions, they often assume similar morphologies:

- Both great apes and humans exhibit wide interindividual variation in the depth of the endocranial imprints that delimit BC inferiorly. Based on imprint depth alone, it is not possible to clearly discriminate between the presence of *fo* versus *lo* in fossil endocasts.
- Furthermore, sulcal ramification patterns in the brain regions underlying BC are variable in both groups (13, 88), such that the association of individual endocranial imprints with specific cerebral sulci often remains ambiguous.
- Also, cerebral structures underlying the BC region are not consistently reproduced as endocranial imprints, and tend to interfere with non-brain imprints. For example, the human ascending ramus *R* (see main Fig. 1B) largely coincides with the inferiormost portion of the coronal suture and/or the base of the anterior ramus of the middle meningeal artery.

As a consequence, in fossil endocasts, frontal lobe organization cannot be reliably inferred from the morphology and structure of the BC region alone. However, the topographical relationships of neurocranial and brain structures in the frontal lobe region as a whole are clearly distinct between great apes and humans (Fig. 1) (34, 35): In all great apes, the precentral sulcus (*pc*) crosses the coronal suture (CO) such that its superior part (*pcs*) is posterior to CO, and its inferior part (*pci*) is situated anterior to it (Fig. 1A). In contrast, in humans, both *pcs* and *pci* are situated on the posterior side of CO (Fig. 1B). Cranio-cerebral topography (17, 89-91) can thus be used as a reliable indicator of frontal lobe organization.

We define the following criteria to discriminate between primitive (ape-like) and derived (human-like) craniocerebral topographies in the frontal lobe region of fossil endocasts:

- *Criterion 1: Imprints of pc and CO are represented on the endocast.*
  - a) Imprints of *pc* cross CO, such that *pci* is on the anterior side of CO: this situation implies an ape-like morphology, thus primitive organization, of the fronto-orbital region. See Fig. 4, inset graph, orange symbol.



b) Imprints of *pc* do *not* cross CO, such that *pci* is on the posterior side of CO: this situation implies a human-like morphology, thus derived organization, of the fronto-orbital region. See Fig. 4, inset graph, turquoise symbol.

- *Criterion 2: Imprints of pc are not represented on the endocast, but CO is represented.*

5 In this situation, topographical relationships between the precentral sulcus, the frontal sulci, and the coronal suture that are consistent across taxa must be considered. In both human and great ape brains, the frontal sulci exhibit substantial variation in ramification patterns. As an effect, individual sulci at mid-height of the frontal cortex are variably identified as representing a middle frontal sulcus (*fm*) proper, or forming part of the inferior (*fi*) versus superior (*fs*) frontal sulci (13). Frontal sulci typically reach the precentral sulcus, but they never cross this structure. As an effect, the posterior delimitation of the frontal sulci defines the anteriormost location of the precentral sulcus. Based on these observations, it is possible to characterize the following topographies:

15 a) Imprints of *fi* and *fm* touch or cross CO: this situation implies that *pci* (even if not visible as an imprint) is located on the posterior side of CO, and that the fronto-orbital region exhibits a human-like morphology, thus derived organization, of the fronto-orbital region. See Fig. 4, inset graph, turquoise symbol.

20 b) Imprints of *fi* and *fm* fade before reaching CO, while imprints of *pci* are not visible: this situation implies that *pci* likely coincides with the location of CO, which represents an intermediate morphology of the fronto-orbital region. Because intermediate morphologies are clearly different from ape-like morphologies, they represent a derived organization of the fronto-orbital region. See Fig. 4, inset graph, grey symbol.

25 - *Criterion 3: Discrimination between endocranial imprints of the inferior precentral sulcus (pci) and imprints of bony elevations along the coronal suture.*

30 On human and great ape endocasts, the fronto-orbital region between Broca's Cap (BC) and the coronal suture (CO) often exhibits a combination of sulcal imprints, and imprints caused by raised bone margins (lipping) along CO. In fossil hominin endocasts, CO lipping can thus potentially be confounded with the imprints of a *pci* situated anterior to the coronal suture. These ambiguities can be resolved as follows:

a) Primitive condition: on great ape endocasts, imprints of *pci* course toward BC and often bisect its superior region but do not reach its inferior border (Fig. 1A).

- b) Derived condition: on human endocasts, imprints caused by lipping along the borders of CO are located posterior to BC, and typically extend downward to the level of the inferior border of BC (see e.g. fig. S3).

5

#### M4. Geometric morphometric analysis of endocranial shape

Endocranial shape was quantified with  $K=921$  three-dimensional anatomical landmarks (LMs), which are distributed equally over the entire surface of the endocast, and represent fixed point  
10 LMs ( $K_p=27$ ), curve semilandmarks (SLMs) ( $K_c=110$ ), and surface SLMs ( $K_s=784$ ). Fixed LMs and curve SLMs were acquired with Avizo. A template of regularly-spaced surface SLMs was defined for one specimen, then warped to every other specimen, using the fixed LMs and curve  
15 SLMs as nodes of a thin-plate spline (TPS) interpolation function, and projecting the warped surface SLMs onto the target specimens along endocranial surface normals. To optimize the position of SLMs and establish geometric correspondence across all specimens of the sample, the curve SLMs were allowed to slide along tangents to the curves, and the surface SLMs along  
20 tangents to the surface. Sliding was iterated until convergence to the minimum bending energy criterion (92). Since natural patterns of left-right asymmetry are not considered here, all specimens were symmetrized via relabeled reflection of landmarks. Finally, Generalized Procrustes Analysis (GPA) was applied to minimize differences in scale, position and orientation  
between the specimens' landmark configurations. Principal Components Analysis (PCA) of shape was then applied to the Procrustes-aligned specimens to explore and visualize major patterns of shape variation in the sample (Fig. 3). All procedures were performed with the R  
package Morpho (93).

25

#### M5. Computing and visualizing endocranial shape change associated with the transition from primitive to derived frontal lobe organization

30 Endocranial shape change in early *Homo* associated with the transition from primitive to derived organization of the frontal lobe (see Fig. 4) was evaluated by computing the mean endocranial shapes of the two respective samples (specimens representing the primitive organization: KNM-ER 1805, KNM-ER 1813, KNM-ER 3733, KNM-WT 15000, D2280, D2700, D3444, and D4500; specimens representing the derived organization: KNM-ER 3883, Sangiran 17,  
35 Sambungmacan 3,4, Bukuran, Solo 1,5,6,9,10,11, and ZKD XII). A Procrustes ANOVA test for between-group differences in endocranial shape yielded a  $p$ -value of 0.019 [R package Geomorph v3.1.2 (94)]. Shape change from primitive to derived mean endocranial morphology

was visualized (see Fig. 4B) as above-average expansion (positive size allometry) of local endocranial surface regions, both in terms of local outward movement of the surface (bulging), and of local surface area increase, using the methods described in ref. (95).

5

## Supplementary Text

### S1. Morphology of the Dmanisi endocasts

10 The CT-based descriptions of the endocranial morphology of the five Dmanisi crania focus on the following aspects: 1) state of preservation; 2) overall shape and petalial asymmetry; 3) cerebellar fossa morphology and position; 4) imprints of cortical sulci and gyri (from anterior to posterior) and cranio-cerebral topography; 5) imprints of venous sinus structures.

15 The endocast of the adult individual **D2280** (fig. S1A) is generally well preserved, but lacks parts of the basicranial region. It has a rounded overall shape, with a comparatively wide anterior cranial fossa (indicating wide frontal lobes) and right occipital/left frontal petalia. The cerebellar fossa is large and bulges inferiorly. Imprints of the frontal sulci on both left and right sides course toward the precentral sulcus. The precentral sulcus courses from a location near the apex of the endocast in antero-inferior direction towards Broca's Cap (BC). During its course it  
20 crosses the coronal suture at mid-height, such that its inferior portion lies anterior to the coronal suture.

On the left side, a sulcal imprint anterior to the inferior portion of the lambdoid suture is labeled (*L*) in fig. S1A. Assuming a primitive organization of the parieto-occipital cortex of the Dmanisi hominins (see Results and Fig. 4), this imprint could represent a remnant of a great ape-like lunate sulcus (*L*).  
25

The apical parietal region of the endocast exhibits marked bilateral keeling, indicating a wide superior sagittal venous sinus. The venous draining system is further characterized by a dominant left transverse sinus, a curved left sigmoid sinus located at the anterior border of the cerebellar fossa, and weakly expressed occipital marginal sinuses on both sides of the foramen magnum.  
30

The cranium of the adult individual **D2282** (fig. S1B) is fragmentary and exhibits substantial taphonomic distortion, which required digital retrodeformation and reconstruction. Several key endocranial structures are nevertheless visible. Similar to D2280, the endocranium is rounded and exhibits wide frontal lobes. The cerebellar fossae are only moderately bulging. Petalial  
35

asymmetry cannot be ascertained. On the better-preserved left side, the precentral sulcus crosses the coronal suture at mid-height and courses toward the center of BC. On the left side, a sulcal imprint at the antero-inferior border of the lambdoid suture could represent a remnant of *L* (assuming a primitive organization of the parieto-occipital cortex). Bilateral sagittal keeling indicates a wide superior sagittal sinus. The transverse sinus on the right side likely represents the dominant one.

The neurocranium of the adolescent individual **D2700** (fig. S1C) is well preserved externally but less so internally. Parts of the neurocranium were missing *in situ*, while endocranial features representing the frontal cortex were partly damaged during an early attempt at physical casting. Furthermore, structural detail in the parietal and occipital region of the endocast is blurred by a thin but dense calcite layer, which tightly adheres to the bone surface.

In lateral and posterior views, the endocast appears rounded; in superior view, it presents a marked pre-coronal constriction, a feature that is often seen on endocasts of Asian *H. erectus*. The endocast exhibits left frontal petalia. The occipital poles are moderately projecting. The cerebellar fossae are only moderately bulging. Endocranial imprints of the frontal sulci are weak compared to the other Dmanisi specimens. On both sides, the imprint of the medial frontal sulcus courses toward the coronal suture, where it approaches the precentral sulcus. The inferior portion of the precentral sulcus lies in front of the coronal suture and courses toward BC. Preservation of the endocranial base region permits estimation of cranial base angulation. The cranial base angle between landmarks basion, sella, and foramen caecum is 135° [CBA1 (36)]. The angle between the clivus plane and the midplane of the anterior cranial fossa (planum sphenoidale) is 124° [CBA4 (36)]. These values are at the upper end or above the range of variation of modern humans of similar dental age [CBA1: 132-137°; CBA4: 106-118° (37)].

The superior sagittal sinus is represented by a marked, narrow imprint with drainage into both left and right transverse sinuses, with the right side being the dominant one. The sigmoid sinus is comparatively straight (rather than recurved). Occipital marginal sinuses are expressed on both sides.

The endocranial cavity of the edentulous cranium **D3444** (fig. S1D) was only partially filled with matrix *in situ* (31), indicating rapid sedimentation. The endocranial surface suffered some taphonomic damage, such as dislocation of the left temporal pyramid, and loss of parts of the anterior cranial base and of the internal table on the left fronto-parietal region. The endocast has a globular shape that is similar to that of some modern human endocasts (see main Fig. 3).

However, it exhibits pre-coronal constriction similar to D2700. The endocast exhibits slight right frontal petalia. The frontal sulci are represented by marked endocranial imprints, which course

toward the imprint of the precentral sulcus. The inferior part of the precentral sulcus lies anterior to the coronal suture, and courses toward the center of BC. The superior sagittal sinus drains into the dominant right transverse sinus. The sigmoid sinus curves around the anterior region of the cerebellar fossa. On the right side, it drains into the occipital marginal sinus.

5

Cranium **D4500** and mandible D2600 represent the most complete skull of early *Homo* found to date. The endocast is fully preserved, except a minimal area of the internal table in the occipital region (fig. S1E). Like in D2700 and D3444, the endocranial cavity of D4500 was only partly filled with sediment *in situ*. Sediment adhering to the middle and anterior cranial fossae was removed using synchrotron imaging and semi-automated image segmentation procedures. In superior view, the D4500 endocast exhibits right-occipital petalia and associated Yakovlevian torque, as expressed by the lower position of the right compared to the left cerebellar fossa. Pre-coronal constriction is marked, but the frontal lobes remain relatively wide. Complete preservation of the internal cranial base permits direct measurement of cranial base angles CBA1=156° and CBA4=144°.

10

15

The frontal sulci are represented by marked imprints; they course toward the precentral sulcus, which is clearly represented on both sides of the endocast. The inferior precentral sulcus is located just anterior to the coronal suture and courses inferiorly toward BC. In posterior and superior views, sulcal imprints anterior to the lambdoid suture and running approximately parallel to it are visible on left and right sides of the endocast. Assuming a primitive organization of the parieto-occipital cortex, these imprints potentially represent remnants of *L* that communicated with the posterior ends of the intraparietal sulci.

20

25

The superior sagittal sinus is represented by a marked midsagittal imprint, and bilateral keeling indicates the attachment sites of the cerebral falx. Also, the parieto-occipital region exhibits several Pacchionian depressions. Imprints of the transverse sinuses are inconspicuous. The sigmoid sinus follows a straight course along the anterior portion of the cerebellar fossa. On the right side, a marked occipital marginal sinus is present.

#### *Petalial patterns in the Dmanisi sample*

30

Petalial asymmetry was scored in the four well-preserved Dmanisi specimens D2280, D2700, D3444, and D4500 (see Table 1). While the standard petalial pattern of great apes and humans is left-occipital/right-frontal (96, 97), three of the four scored Dmanisi specimens exhibit reversed frontal and/or occipital petalia (D2280: right-occipital/left-frontal; D2700: left-frontal; D4500: right-occipital), and we may ask whether their prevalence is unusually high. Using the petalial frequencies published in ref. (96) we can estimate the probability *p* of finding by chance at least 2 right-occipital and at least 2 left-frontal petalia in a sample of *N*=4 specimens: *p*=16%. In

35

statistical terms, this is reasonably large to conclude that the number of petalial reversals seen in the Dmanisi sample is likely an effect of random sampling.

5 S2. Endocranial morphology of early *Homo* from Africa

Unless otherwise stated, all descriptions are based on CT scans of the original fossil specimens.

*KNM-ER 1805*

10 The endocranial morphology of this specimen has been described as exhibiting “a pongid-like fronto-orbital sulcus” (21). Examination of the frontoparietal endocranial region shows imprints representing the right and left precentral sulci, which cross the coronal suture at mid-height (fig. S2A). This supports Falk’s original interpretation (21), and provides additional evidence for a primitive organization of the frontal lobe in this specimen.

15

*KNM-ER 1813*

The left and right frontoparietal endocranial regions of this specimen exhibit sulcal imprints that can be associated with the inferior frontal and precentral sulci, respectively (fig. S2B). The latter structures extend from postero-superior to antero-inferior, crossing the coronal suture at mid-  
20 height, and coursing toward Broca’s Cap. This topography implies that Broca’s Cap is delimited inferiorly by the fronto-orbital sulcus, thus indicating a primitive organization of the inferior frontal lobe.

*KNM-ER 1470*

25 According to Falk (21) this specimen provides key evidence for a derived organization of the frontal lobe (fig. S2C): endocranial structures on the left anterior surface have been interpreted as imprints of the inferior frontal sulcus and parts of the anterior (=horizontal, *R*) and ascending (=vertical, *R'*) rami of the lateral (Sylvian) sulcus, respectively. The latter two structures (*R'* and *R* in fig. S2C) would indicate that the Broca Cap region of KNM-ER 1470 comprised pars  
30 orbitalis and pars triangularis, and therefore exhibited a modern human-like organization. CT-based re-examination of the endocranial morphology reveals that structure *R* likely is a taphonomic defect (in humans, the ascending ramus largely coincides with the lowermost part of the coronal suture; see main Fig. 1B).

35 Since imprints of the precentral sulci are not present on this specimen, structure *R'* (and its superior extension: stippled line in fig. S2C) remains ambiguous: it could represent a human-like anterior horizontal ramus of the lateral sulcus (21), or an ape-like subcentral anterior sulcus (13).

Overall, the frontoparietal region of the KNM-ER1470 endocast exhibits little structural detail, such that inferences on the location and course of the precentral sulcus cannot be drawn with certainty.

5 *KNM-ER3733*

This cranium exhibits extensive fragmentation as well as local taphonomic distortion. Also, parts of the anterior cranial fossa are still filled with matrix. CT-based examination indicates that various endocranial imprints are spatially associated with fractures. As an effect, imprints cannot definitely be assigned to brain structures versus taphonomic damage. On both sides, endocranial imprints situated anterior to the coronal suture and coursing in supero-inferior direction likely represent the inferior precentral sulcus, as it is located immediately superior (rather than posterior) to BC (see criterion 3a) (fig. S2D). These topographical relationships would indicate that Broca's Cap is delimited inferiorly by a fronto-orbital sulcus, reflecting a primitive organization of the fronto-orbital cortex.

15

*KNM-ER 3883*

The neurocranium of this specimen exhibits taphonomic damage, such that endocranial imprints only partly represent brain sulci, while others result from fragment displacement and indentation, especially on the left side (fig. S2E). On the right side, an imprint in the parietal area likely represents a portion of the central sulcus. A shallow imprint immediately anterior to the inferior portion of the coronal suture, but posterior to BC likely reflects marked lipping of the frontal squama along the coronal suture (see fig. S2E, hatched area). Imprints of the middle and inferior frontal sulci (*fm*, *fi*) reach the anterior side of the imprint of the coronal suture, indicating that *pci* was located beneath or posterior to the suture. Considering the location of the central sulcus on this endocast confirms that the precentral sulcus must have been located in close vicinity to the coronal suture. Together, the frontal region of this endocast is thus best interpreted as exhibiting a morphology that is intermediate between great ape-like and human-like cranio-cerebral topographies.

20

25

30

*KNM-WT 15000*

The cranium of this specimen has been reconstructed from several fragments (60). Partial mismatch between fragments is likely due to local taphonomic distortion. The left side of the endocast is better preserved and exhibits more structural detail than the right side (fig. S2F). A faint imprint anterior to the coronal suture likely represents the inferior precentral sulcus, as it is coursing toward the center of BC. This indicates a primitive organization of the inferior frontal lobe.

35

*KNM-ER 42700 (Ileret)*

CT-based visualizations of the reconstructed endocast provided in ref. (62) have a low spatial resolution, thus revealing relatively little structural detail. On the left inferior frontal region, an imprint representing the inferior frontal sulcus (*fi*) courses in postero-superior direction to reach the coronal suture. This configuration implies that *pci* must have been located posterior to this suture, indicating a derived organization of the frontal lobe.

*BOU-VP-2/66 (Daka, Bouri)*

The microCT-based visualizations of the endocast of this specimen provided in ref. (63) show various diagnostic features. The imprints of the middle/inferior frontal sulci course in antero-posterior direction to reach the coronal suture. Accordingly, the precentral sulcus must have been located posterior to the coronal suture. Together, these topographical relationships indicate a derived organization of the frontal lobe. Small sulci in the occipital pole region are possibly associated with *L*.

*UA-31 (Buia)*

MicroCT-based visualizations (64) show a smooth endocranial surface with only few imprints representing cerebral sulci. On the left side, imprints of the middle and inferior frontal sulci extend posteriorly to the coronal suture, indicating that the inferior precentral sulcus was located posterior to the suture. As in Daka and Ileret, these topographical relationships indicate a derived organization of the frontal lobe.

S3. Endocranial morphology of early *Homo* from East Asia

The endocranial morphology of early *Homo* from East Asia has been investigated since the early 20<sup>th</sup> Century (98-100), and new evidence and comparative context has been provided in refs. (101, 102). Here we focus on those aspects of endocranial morphology that are relevant for addressing questions of cranio-cerebral topography and frontal lobe organization. Unless otherwise stated, all observations and descriptions reported here are based on new CT scans of the original fossil specimens.

*Mojokerto*

CT-based segmentation of this specimen reveals few endocranial imprints in the frontal region (fig. S3A). The left endocranial surface shows an imprint of the inferior frontal sulcus that



originates above and anterior to Broca's Cap and courses in supero-posterior direction to reach the coronal suture. This implies a post-coronal location of the inferior precentral sulcus (criterion 2a), thus a derived organization of the inferior frontal lobe.

5 *Sangiran 9*

MicroCT-based visualizations of this specimen [see Fig. 2F in ref. (74)] show marked imprints representing the left middle/inferior frontal sulci. On the left side, one imprint corresponding to the middle frontal sulcus crosses the coronal suture. This indicates that the precentral sulcus was situated posterior to the coronal suture.

10

*Sangiran 17*

The well-preserved left side of this specimen shows several endocranial imprints in the frontal region representing the superior, middle and inferior frontal sulci (fig. S3B). These imprints course in approximately horizontal direction toward the coronal suture but tend to fade toward the suture such that it is not possible to ascertain whether they reached or crossed the suture. A faint imprint of the superior precentral sulcus is preserved on the left side. Overall, the most parsimonious interpretation of this pattern is that the inferior precentral sulcus (which did not leave imprints) was located in the close vicinity of the coronal suture.

15

20

*Bukuran*

The Bukuran specimen (77) exhibits marked frontal endocranial imprints (fig. S3C). On the better-preserved left side, imprints representing the inferior, middle and superior frontal sulci reach the coronal suture, indicating that the precentral sulcus was just beneath, or posterior to the coronal suture.

25

*Trinil 2 (Pithecanthropus I) and Sangiran 2 (Pithecanthropus II)*

In Trinil 2, the endocranial imprint representing the right inferior frontal sulcus touches the marked imprint of the coronal suture [see visualizations in refs. (68, 70)]. In Sangiran 2, all imprints representing frontal sulci reach the coronal suture (68). The endocranial topography of both specimens thus indicates that the precentral sulcus was situated posterior to the coronal suture.

30

*Solo (Ngandong) specimens*

We use here the specimen names/numbers of Weidenreich (103), as presented in a synopsis of different naming/numbering systems by Huffman et al. (104). Endocranial surfaces of the Solo specimens are generally smooth, revealing comparatively little structural detail in terms of

35

identifiable sulcal imprints. All specimens exhibit marked thickening (lipping) of the frontal squama in the vicinity of the coronal suture (see fig. S3, hatched areas), resulting in an endocranial depression in the region anterior to the suture. In the endocasts of Solo I and Solo IX the infero-posterior frontal region is only partially preserved, and the few endocranial imprints that can be identified are not diagnostic with regard to frontal lobe organization. Solo II represents an isolated frontal squama; endocranial imprints representing the inferior frontal sulcus touch CO. In Solo V (fig. S3D), the better-preserved left side of the endocast exhibits an imprint of the *fi* that ends at CO. Similar topographic relationships are preserved on the left side of the Solo VI endocast. Solo X reveals various small sulcal imprints on its frontal endocranial surface. Assignment to specific frontal sulci is not attempted here, but it is diagnostically relevant that these imprints are delimited posteriorly by CO. Solo XI preserves an almost complete endocranial surface, which, however, exhibits little structural detail. Traces of the inferior and middle frontal sulci can be identified on both sides; these structures end at the coronal suture.

#### *Sambungmacan 3 and 4*

Endocasts of both Sm3 (fig. S3E) and Sm4 exhibit marked imprints of the frontal sulci, with the inferior frontal sulci extending to CO. Both specimens also exhibit marked endocranial imprints just anterior to CO, but posterior to BC. These imprints are due to bony lipping along the inferior portion of the coronal suture, and do not represent the inferior precentral sulcus (see criterion 3b). Overall, the endocranial topographies of Sm3 and Sm4 indicate a derived organization of the inferior frontal lobe.

#### *Ngawi*

The endocranial cavity of this specimen (82) is well preserved but its morphology is partially obscured by a thin layer of X-ray-dense matrix adhering to the endocranial surface. The left fronto-occipital region exhibits a clear imprint representing the inferior frontal sulcus, which courses in anteroposterior direction to almost reach the coronal suture, likely indicating a frontal lobe morphology where the inferior precentral sulcus coincides with the location of the coronal suture.

#### *Zhoukoudian XII*

CT scans of high-quality casts of this specimen were used to generate a virtual reconstruction (fig. S3F). The endocranial surface of the frontal squama shows marked sulcal imprints. The imprints representing the left and right inferior frontal sulci extend to the coronal suture, indicating that the inferior precentral sulcus was situated posterior to the suture.

## *Hexian*

Photographs and drawings of the endocast of this specimen [see Figs. 3 and 6 in ref. (69)], show imprints representing the right inferior frontal sulcus touching the coronal suture.

5

## S4. Endocranial morphology of Malapa MH1, Dinaledi DH3, and Liang Bua LB1

The endocranial topographies of the small-brained *Australopithecus sediba* (MH1) and *Homo naledi* (DH3) specimens have been reported to bear evidence of incipient fronto-orbital cerebral reorganization. In *Au. sediba* MH1 [ECV 420ccm (10); dated to  $1.977 \pm 0.002$  ma (105), and in *H. naledi* DH3 [ECV 460ccm (9); dated to 0.335-0.236 ma (106)], *pc* crosses CO, thus representing the primitive condition characteristic of *Australopithecus* (7) and early *Homo* (as studied here). Endocranial imprints in the BC region of DH3 have been reported to indicate a derived, human-like configuration of the fronto-orbital region (9). Given its comparatively young geological age, *H. naledi* might thus represent an intermediate frontal lobe organization (9), probably representing a small-bodied/small-brained population derived from a larger-bodied ancestor. However, several observations challenge this interpretation. The inferior precentral sulcus (*pci*) is located anterior to CO, thus indicating a primitive organization of the fronto-orbital region. Also, endocranial imprints in the BC region of DH3 fall within the wide range of variation of sulcal patterning in the corresponding region of chimpanzee brains (13). *H. naledi* might thus represent a group conserving the primitive brain organization characteristic of early *Homo*.

The *H. floresiensis* specimen LB1 [ECV 460ccm (107), dated to 190-50ka (86)] has been described as exhibiting “derived frontal and temporal lobes” [ref. (107), p. 242] indicative of a phylogenetic connection with Southeast Asian *H. erectus*. Although the endocast of LB1 is relatively complete, postmortem fractures, taphonomic distortion and fragment displacement hamper identification of sulcal imprints, especially in the diagnostically relevant inferior frontal region. On the left side, a marked imprint superior to Broca’s Cap is visible on both low-resolution and high-resolution CT-based renderings of the endocast [see visualizations in refs. (85, 107)], possibly representing the left inferior frontal sulcus. The imprint reaches the coronal suture, which would indicate a derived organization of the inferior frontal lobe and provide support for the hypothesis that this taxon represents a late insular form of Southeast Asian *H. erectus* (45). However, the structure coincides with a postmortem fracture at the border of an indented fragment, such that its anatomical identity remains unclear, and inferences on frontal lobe reorganization cannot be based on the criteria defined above.

35

**Fig. S1** (see following pages). Endocranial structures of the Dmanisi crania. **(A)** D2280; **(B)** D2282; **(C)** D2700; **(D)** D3444; **(E)** D4500. Each subfigure is presented in labeled and unlabeled versions. Right/left lateral, anterior/posterior and superior/inferior views. Identified endocranial imprints: red: cerebral sulci; blue: sutures; green: venous sinuses; yellow: meningeal arteries. Abbreviations: CO: coronal suture; LA: lambdoid suture; SA: sagittal suture. Cerebral sulci: *c*: central; *fi*: inferior frontal; *fm*: medial frontal; *fs*: superior frontal; *fo*: fronto-orbital; *ip*: intraparietal; *pc* (*pci*): precentral (inferior); *pt*: postcentral; *ts*: superior temporal; *s*: Sylvian (lateral); (*L*): possible remnants of great ape-like lunate sulcus. Vascular structures: SS: sigmoid sinus; TS: transverse sinus; SSS: superior sagittal sinus; OMS: occipital marginal sinus.

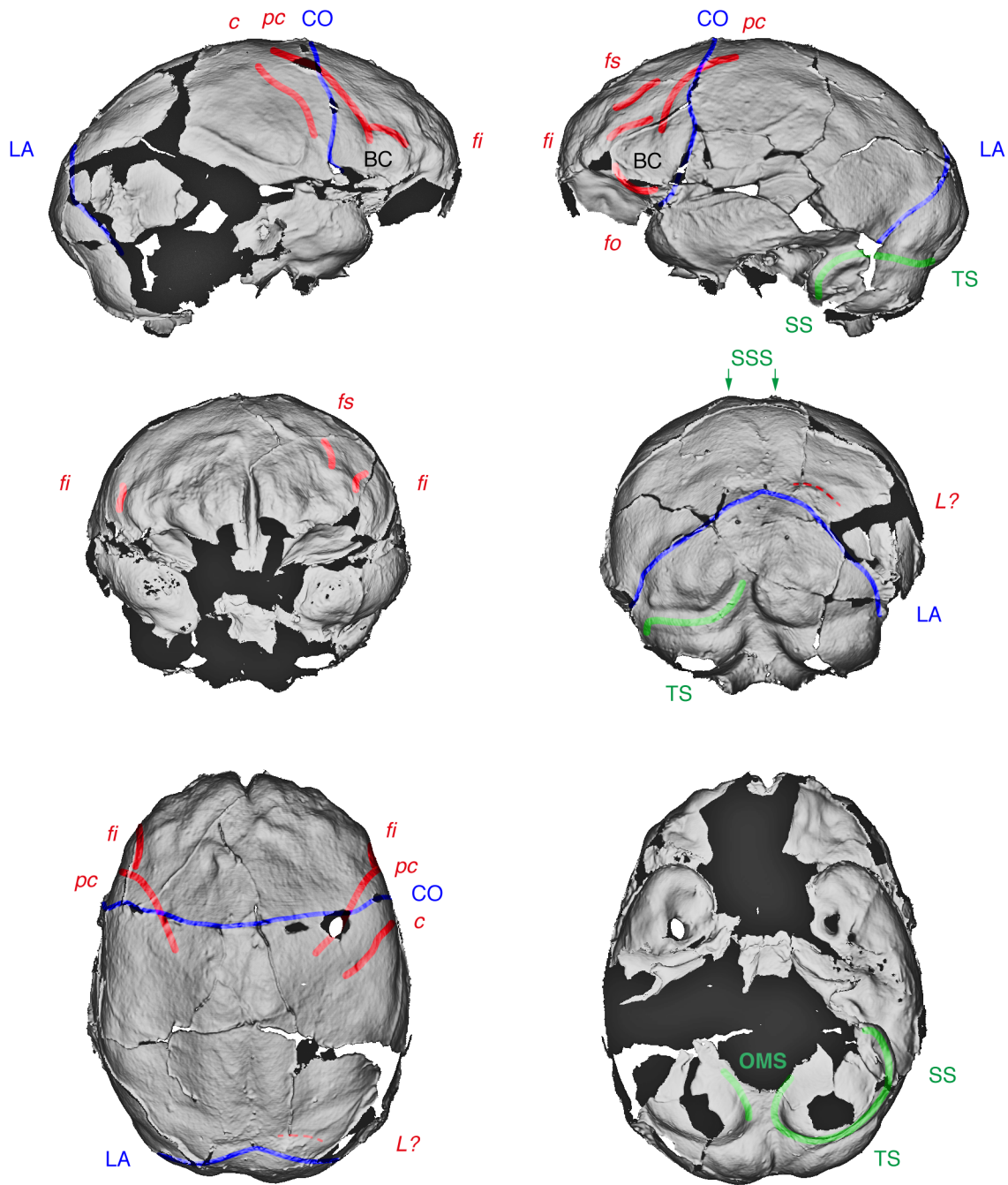


**Fig. S1 A.** Endocranial structures of Dmanisi cranium D2280. Note that the precentral sulcus (*pc*) crosses the coronal suture (*CO*) at mid-height, and courses toward Broca's Cap (*BC*), which is delimited inferiorly by the fronto-orbital sulcus (*fo*). Scale bar is 5 cm. Colors and labels see legend to fig. S1.

5

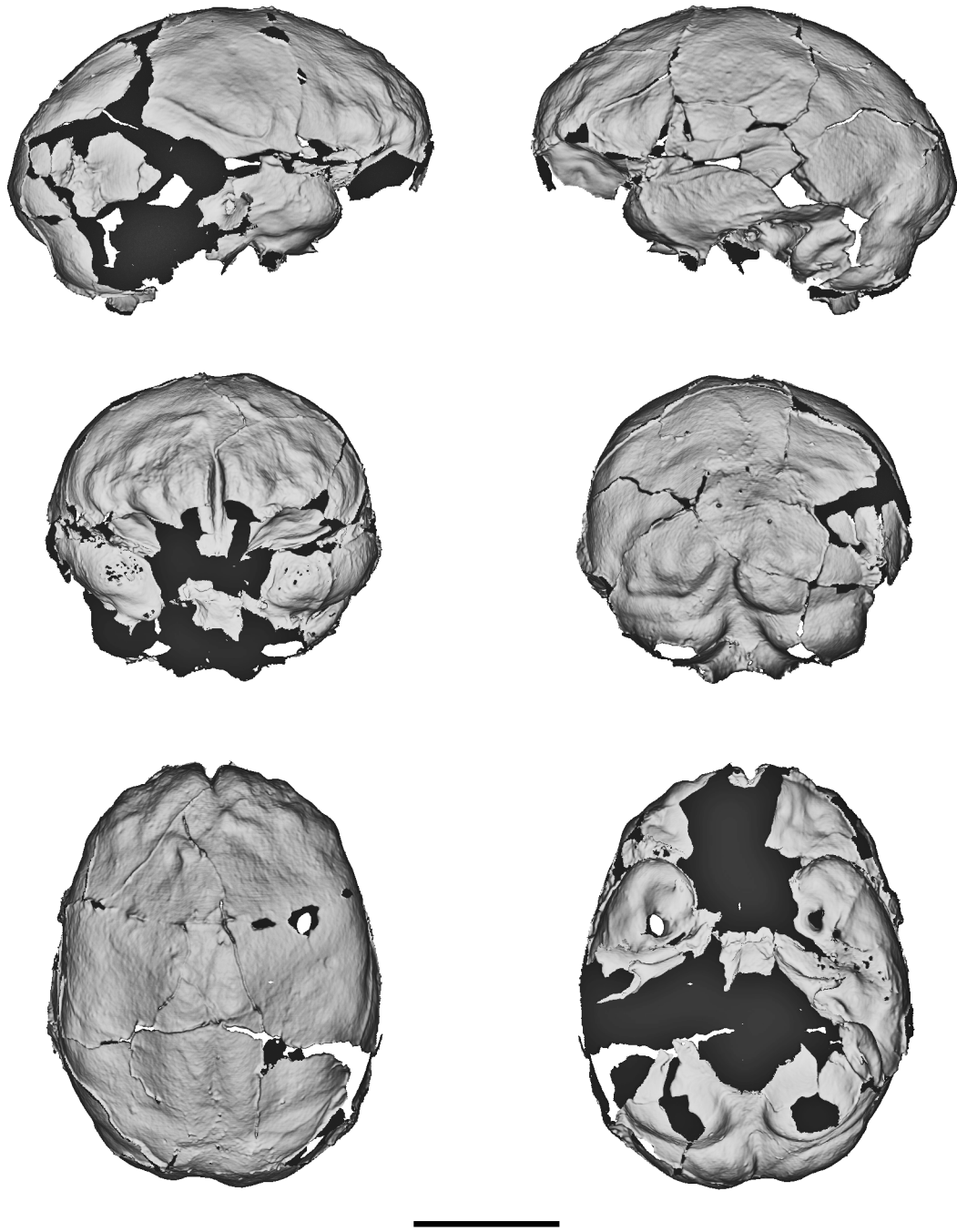


**Fig. S1 A.** Endocranial structures of Dmanisi cranium D2280. Unlabeled 3D reconstruction. Scale bar is 5cm.

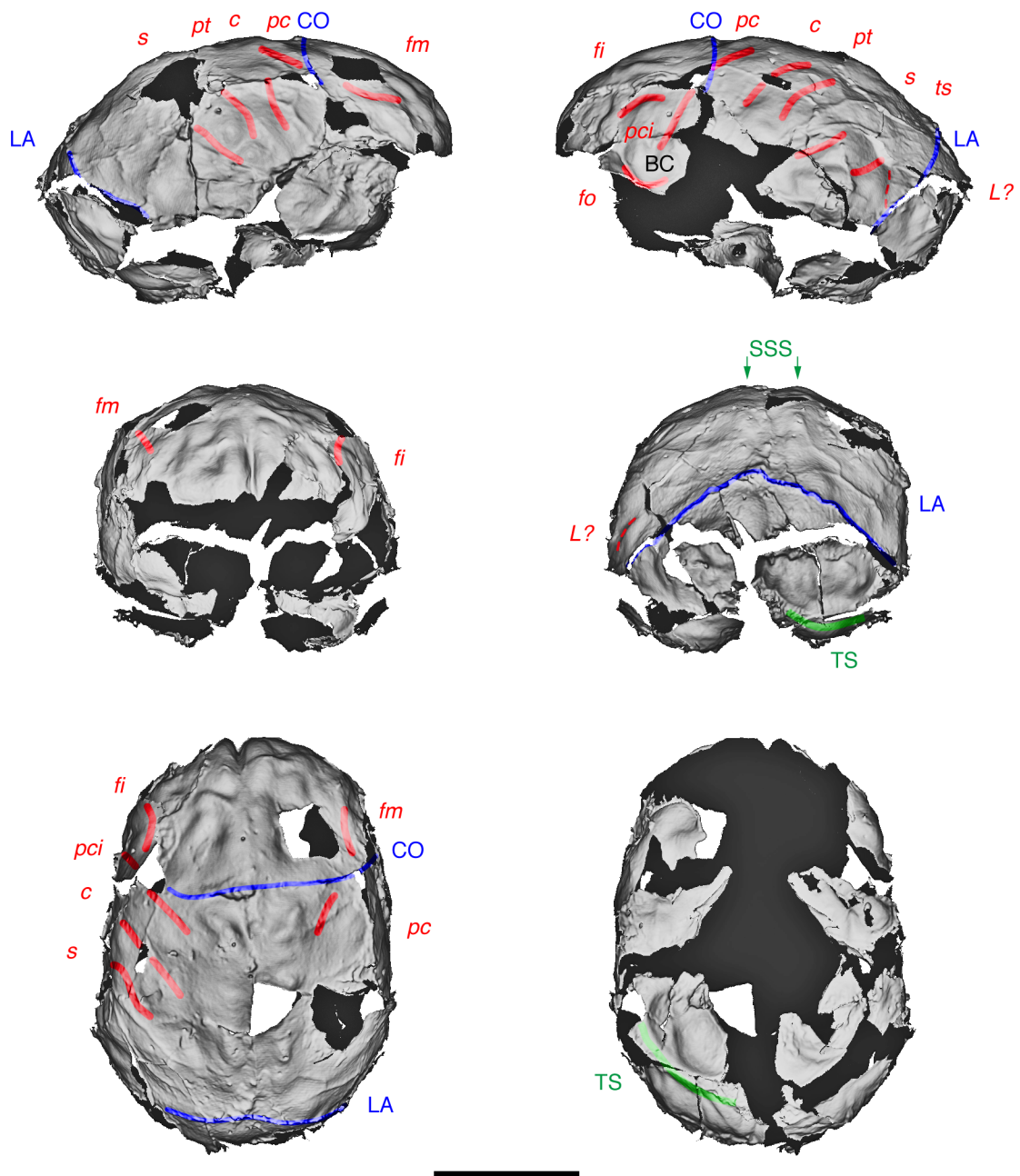


**Fig. S1 B.** Endocranial structures of Dmanisi cranium D2282. Note that the inferior portion of the precentral sulcus (*pci*) is located anterior to the coronal suture (*CO*) and bisects Broca's Cap (*BC*), which is delimited inferiorly by the fronto-orbital sulcus (*fo*). Scale bar is 5 cm. Colors and labels see legend to fig. S1.

5

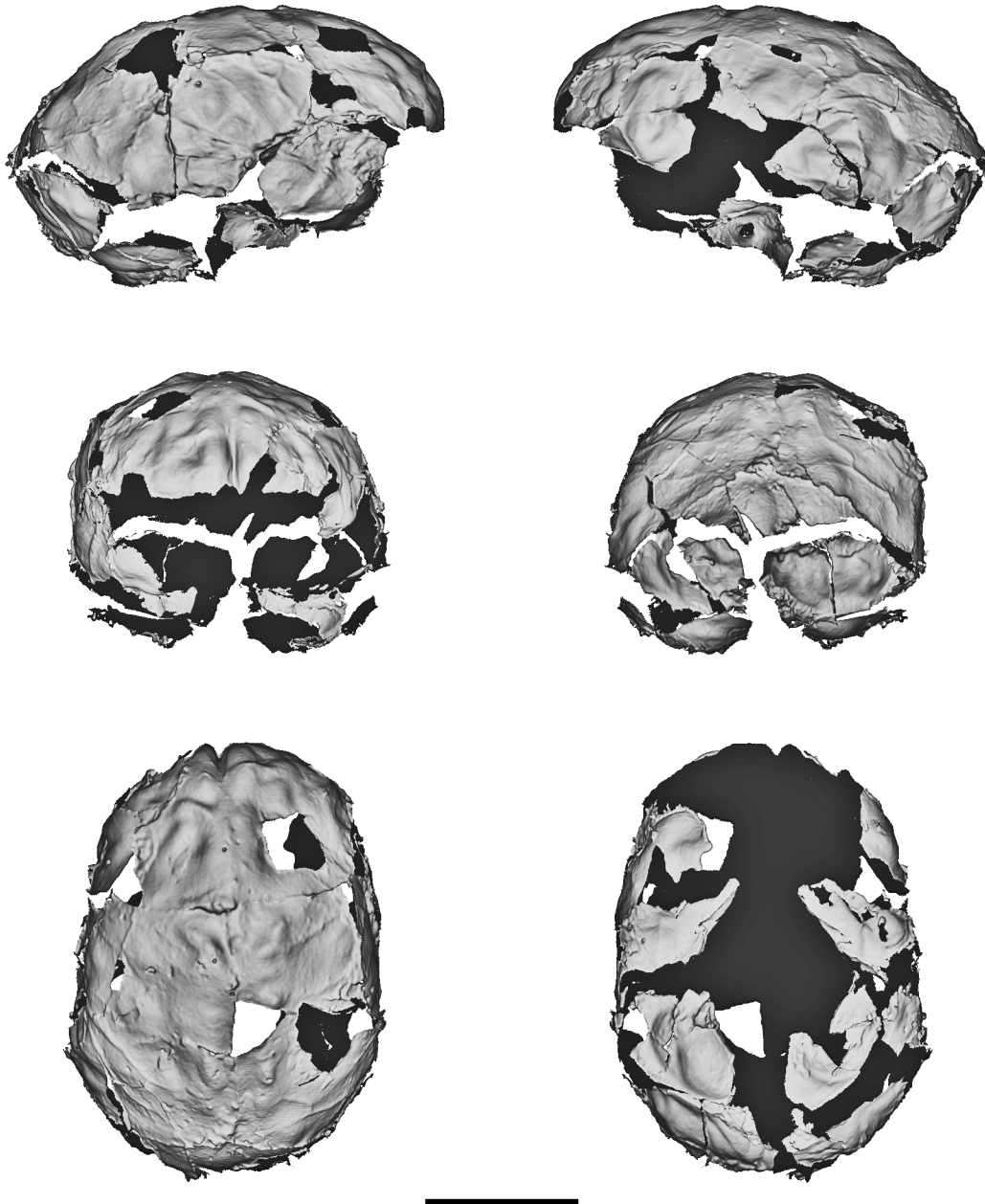


**Fig. S1 B.** Endocranial structures of Dmanisi cranium D2282. Unlabeled 3D reconstruction. Scale bar is 5cm.



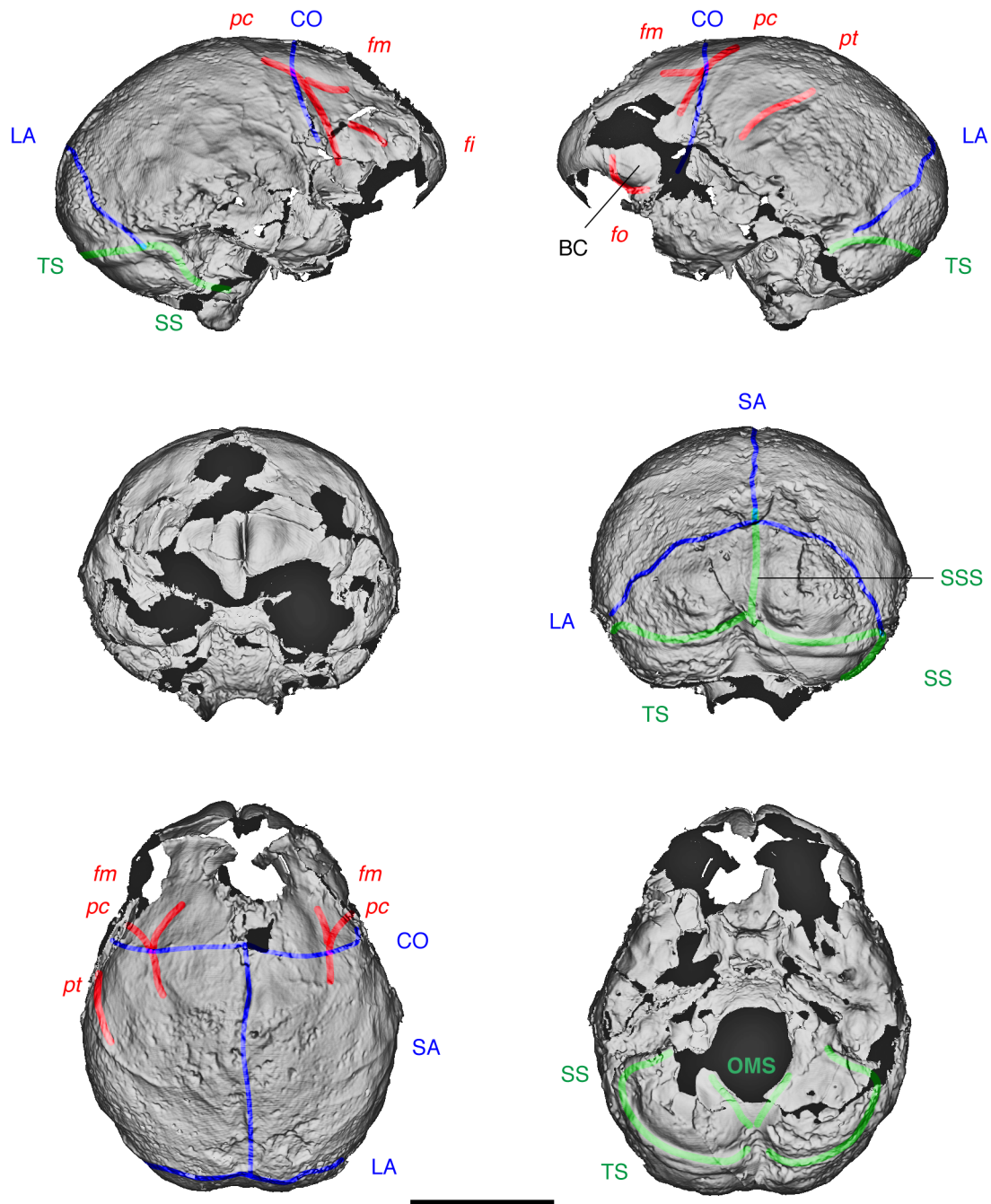


**Fig. S1 C.** Endocranial structures of Dmanisi cranium D2700. Note that the precentral sulcus (*pc*) crosses the coronal suture (CO) at mid-height, and courses toward Broca's Cap (BC), which is delimited inferiorly by the fronto-orbital sulcus (*fo*). Scale bar is 5 cm. Colors and labels see legend to fig. S1.

5

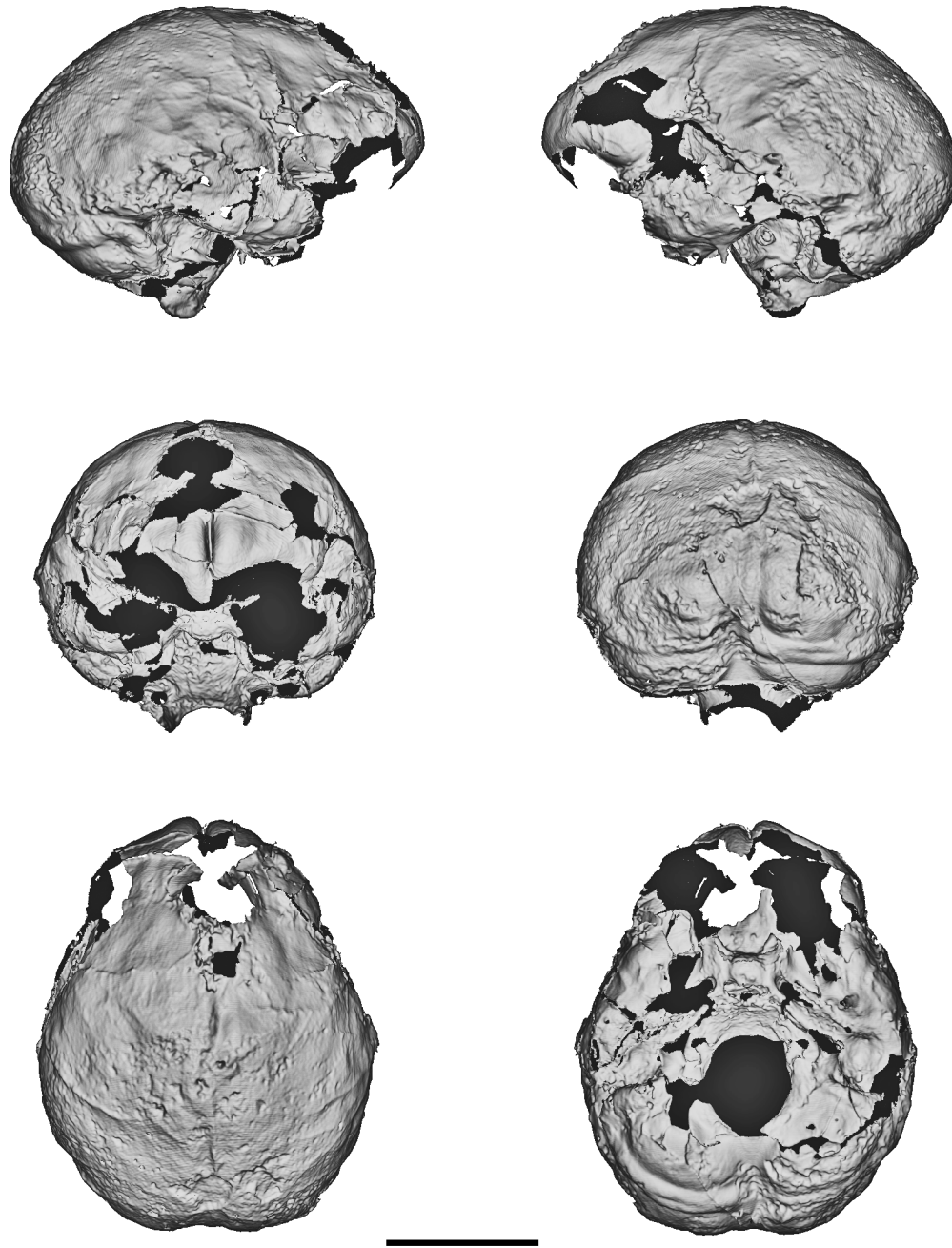


**Fig. S1 C.** Endocranial structures of Dmanisi cranium D2700. Unlabeled 3D reconstruction. Scale bar is 5cm.

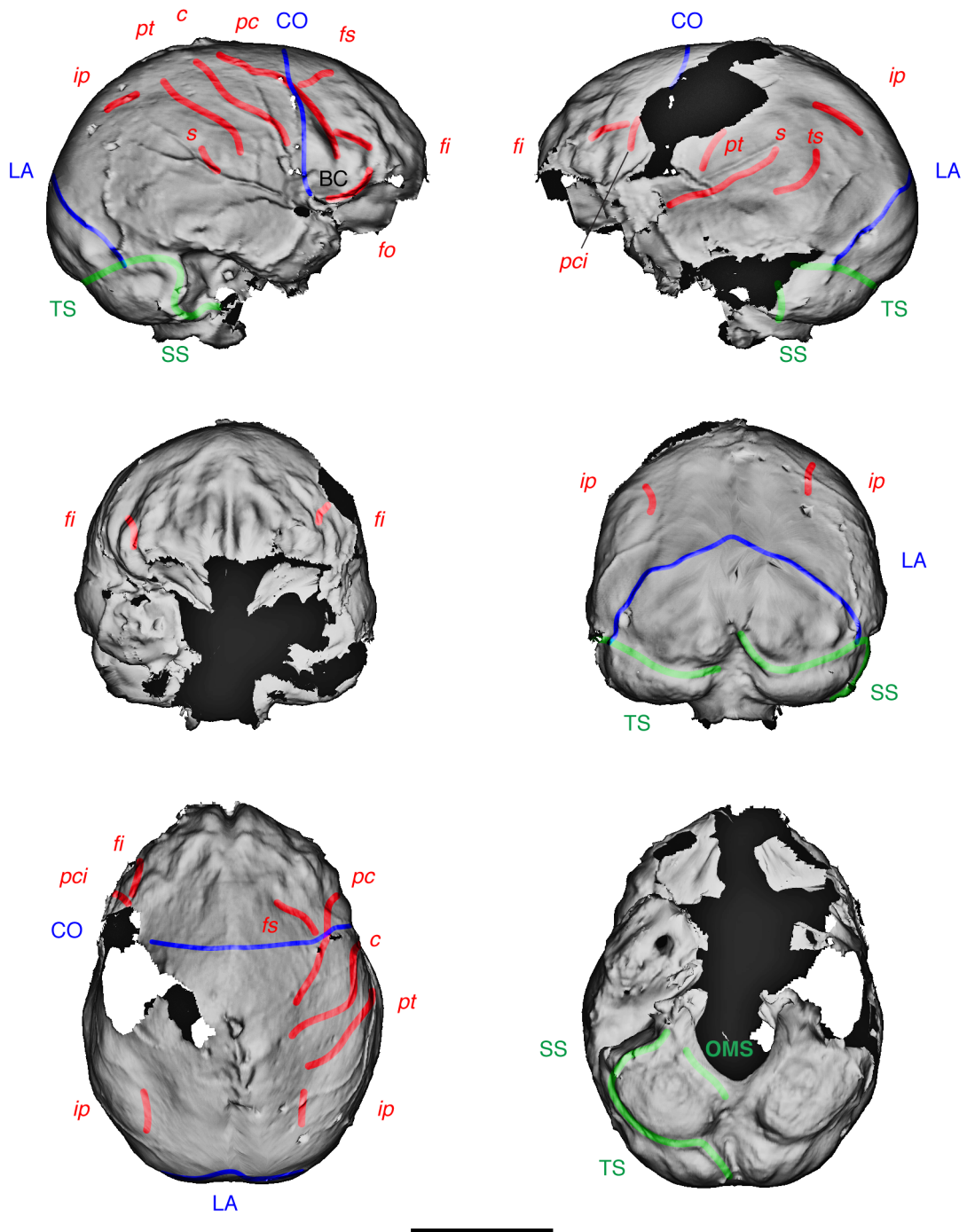


**Fig. S1 D.** Endocranial structures of Dmanisi cranium D3444. Note that the precentral sulcus (*pc*) crosses the coronal suture (CO) at mid-height, and courses toward Broca's Cap (BC), which is delimited inferiorly by the fronto-orbital sulcus (*fo*). Scale bar is 5 cm. Colors and labels see legend to fig. S1.

5

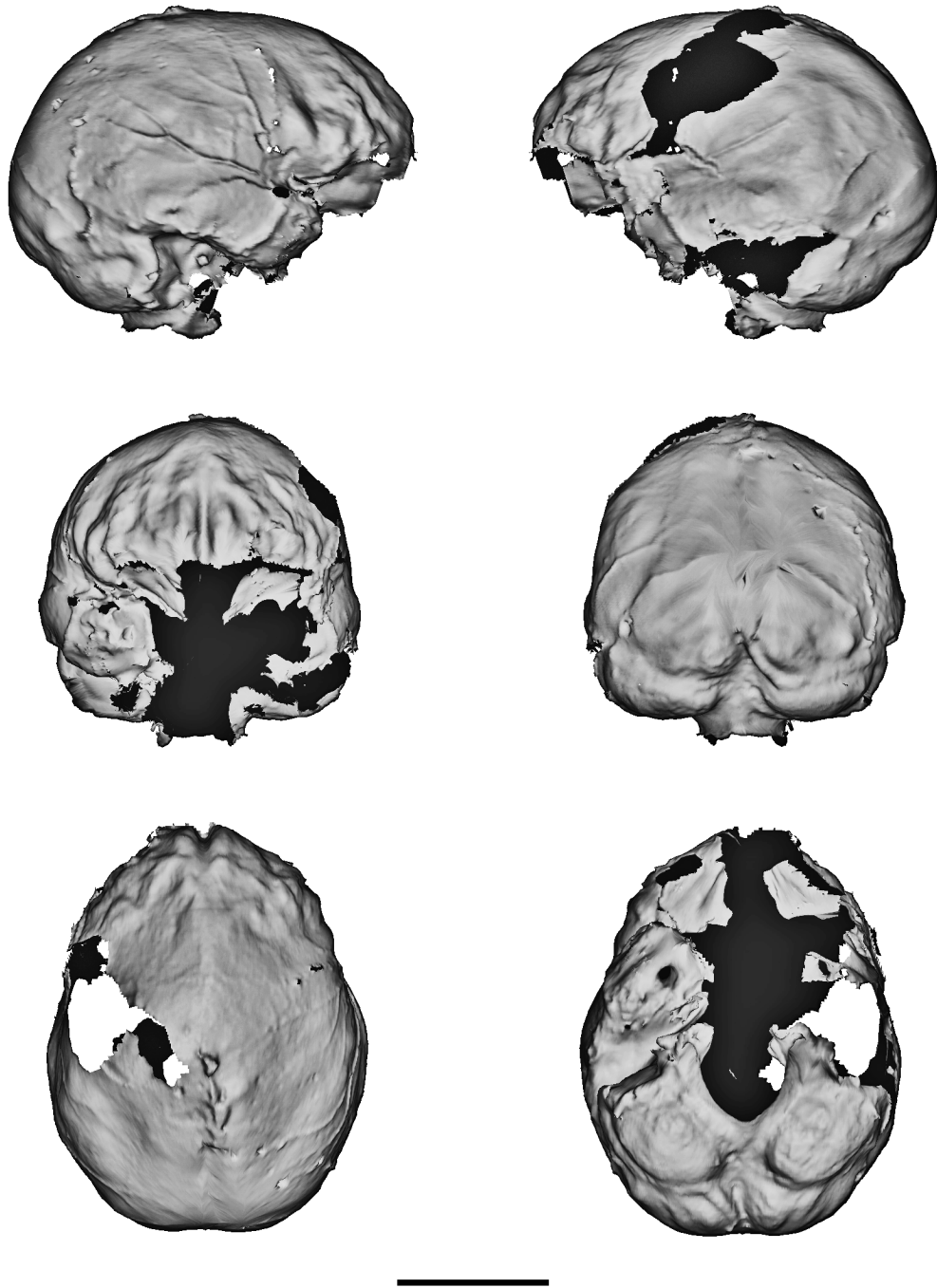
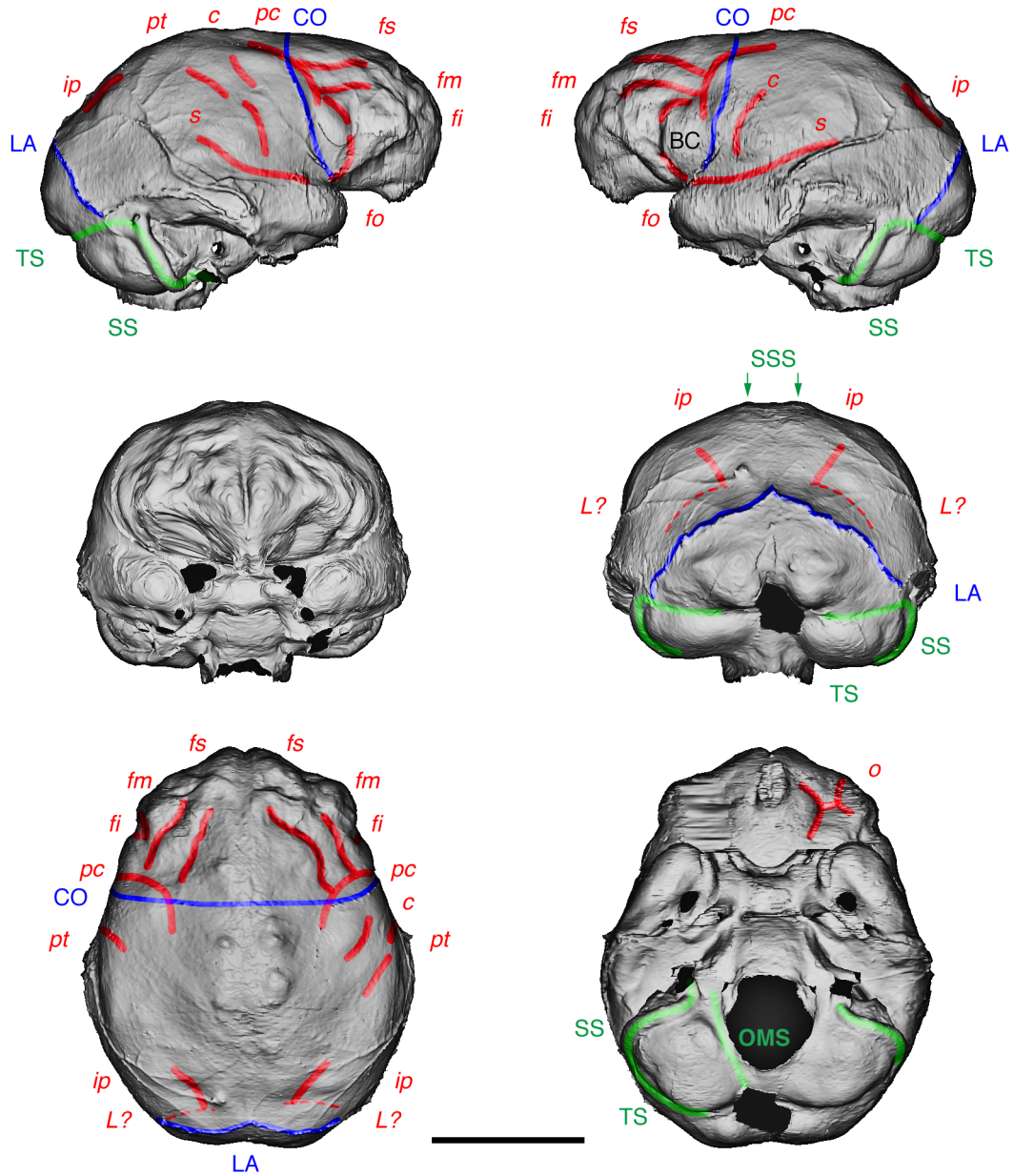


**Fig. S1 D.** Endocranial structures of Dmanisi cranium D3444. Unlabeled 3D reconstruction. Scale bar is 5cm.



5 **Fig. S1 E.** Endocranial structures of Dmanisi cranium D4500. Note that the precentral sulcus (*pc*) crosses the coronal suture (*CO*) at mid-height, and courses toward the postero-superior portion of Broca's Cap (*BC*), which is delimited inferiorly by the fronto-orbital sulcus (*fo*). Scale bar is 5 cm. Colors and labels see legend to fig. S1.

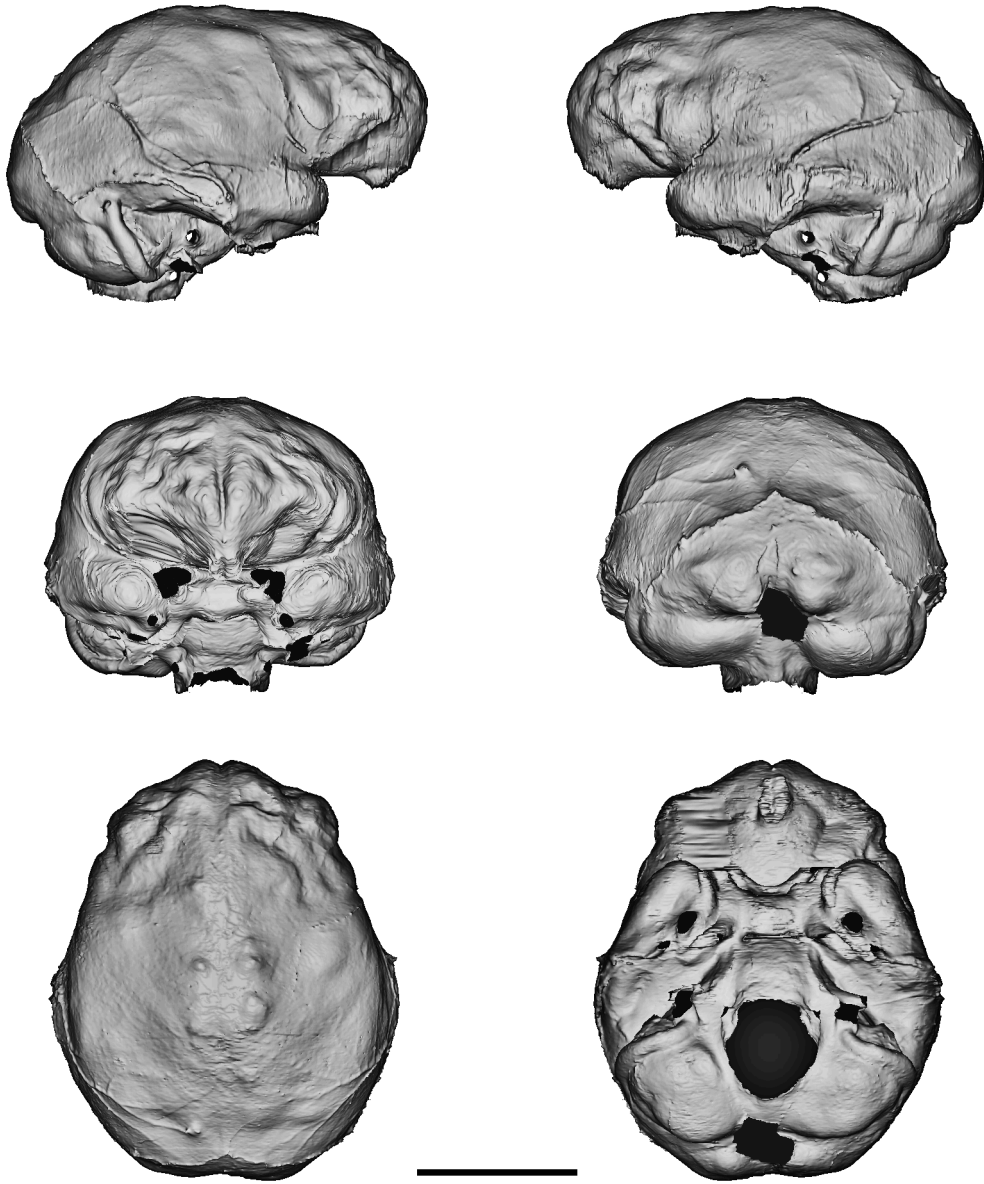
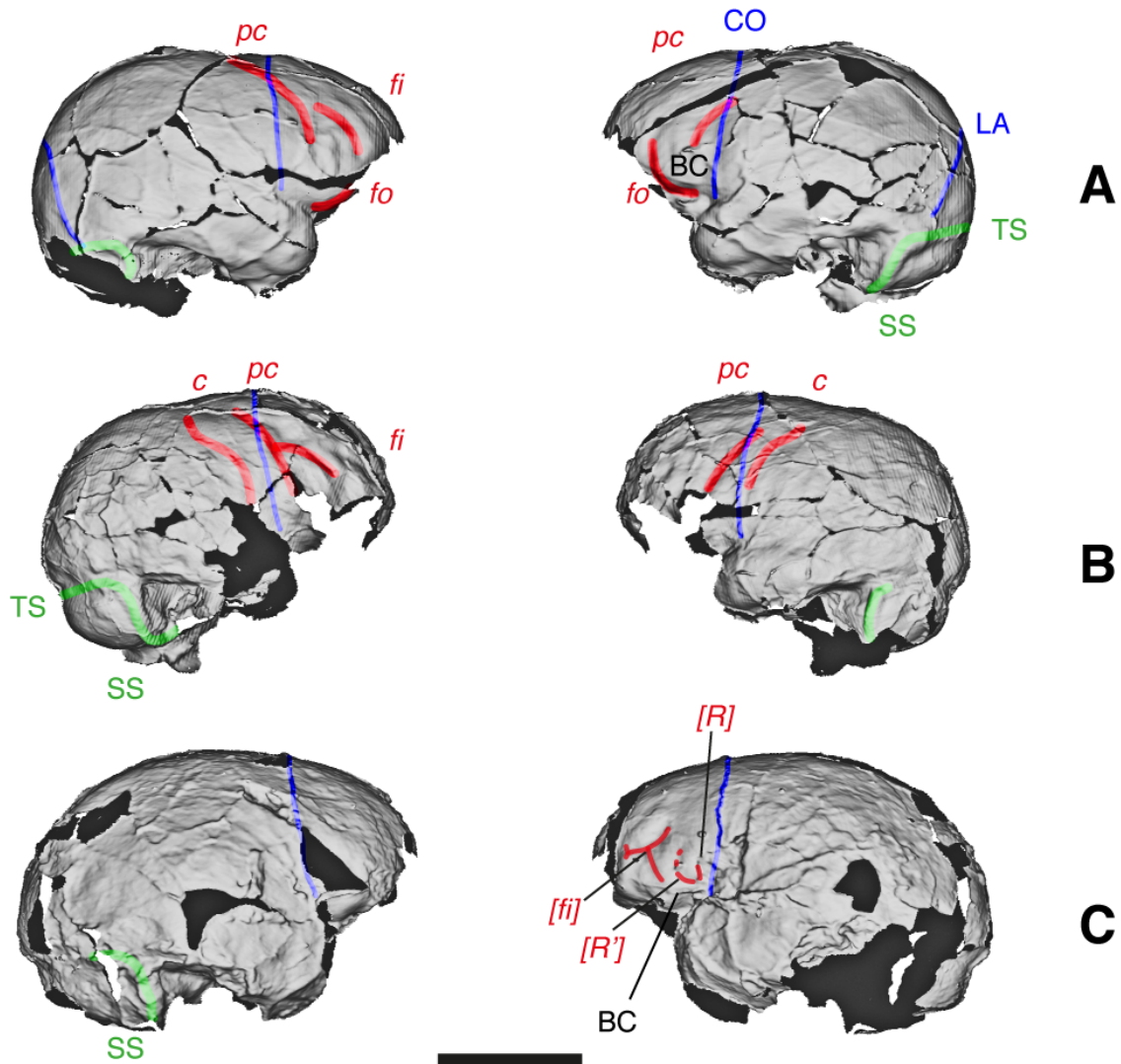


**Fig. S1E.** Endocranial structures of Dmanisi cranium D4500. Unlabeled 3D reconstruction. Scale bar is 5cm.



5 **Fig. S2 A-C.** Endocranial structures of African early *Homo* fossils. (A) KNM-ER 1805; (B)  
 10 KNM-ER 1813; (C) KNM-ER 1470. Colors and labels as in fig. S1. Scale bar is 5 cm. In KNM-  
 ER 1805 (A) the inferior precentral sulcus (*pci*) is situated anterior to the coronal suture (CO)  
 and bisects Broca's Cap (BC). In KNM-ER 1813 (B), the precentral sulcus (*pc*) crosses (CO).  
 The endocast of KNM-ER 1470 (C) is highly fragmented; features labeled in square brackets are  
 represented as in ref. (21).

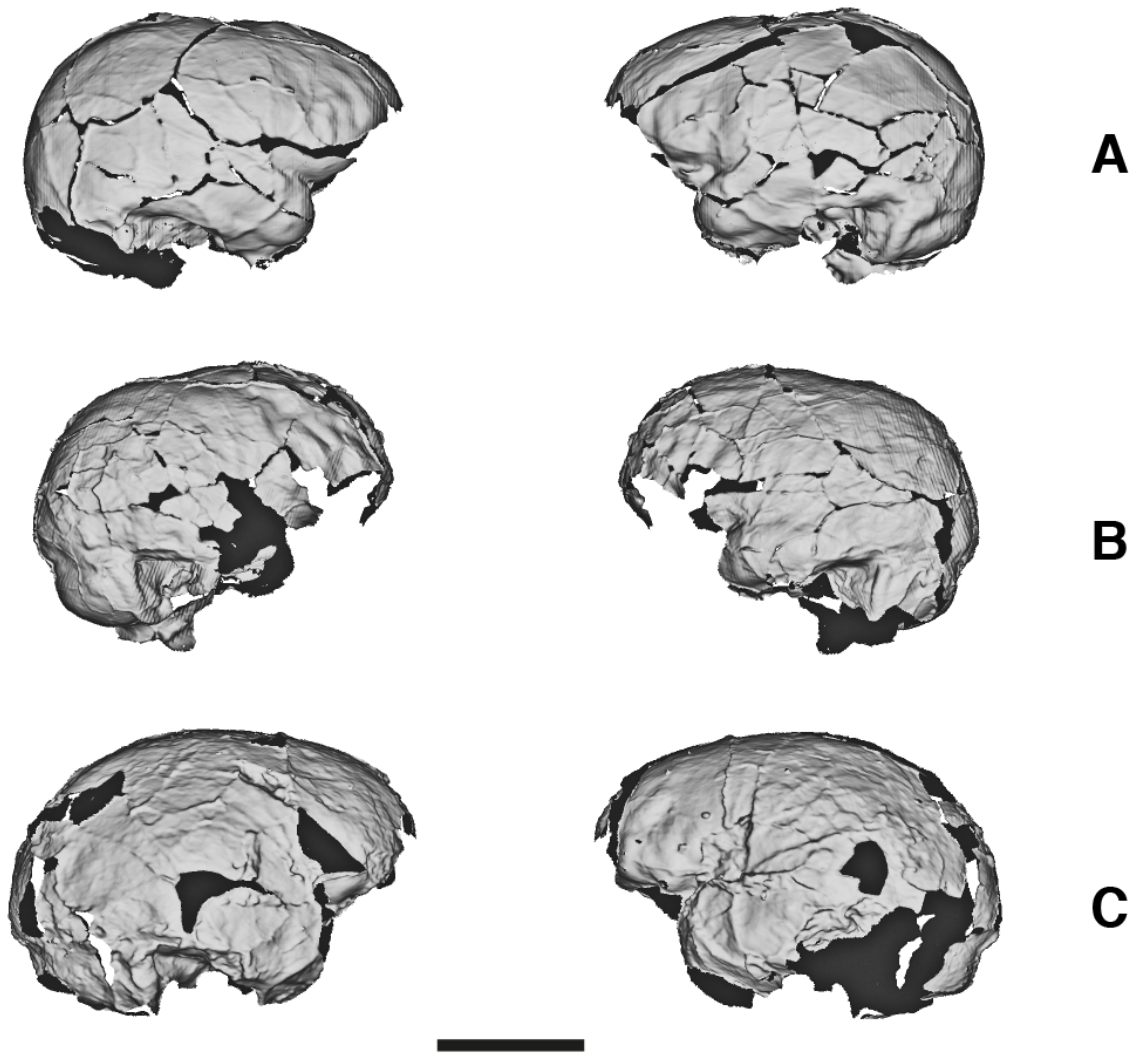


**Fig. S2 A-C.** Endocranial structures of African early *Homo* fossils. (A) KNM-ER 1805; (B) KNM-ER 1813; (C) KNM-ER 1470. Unlabeled 3D reconstructions. Scale bar is 5cm.



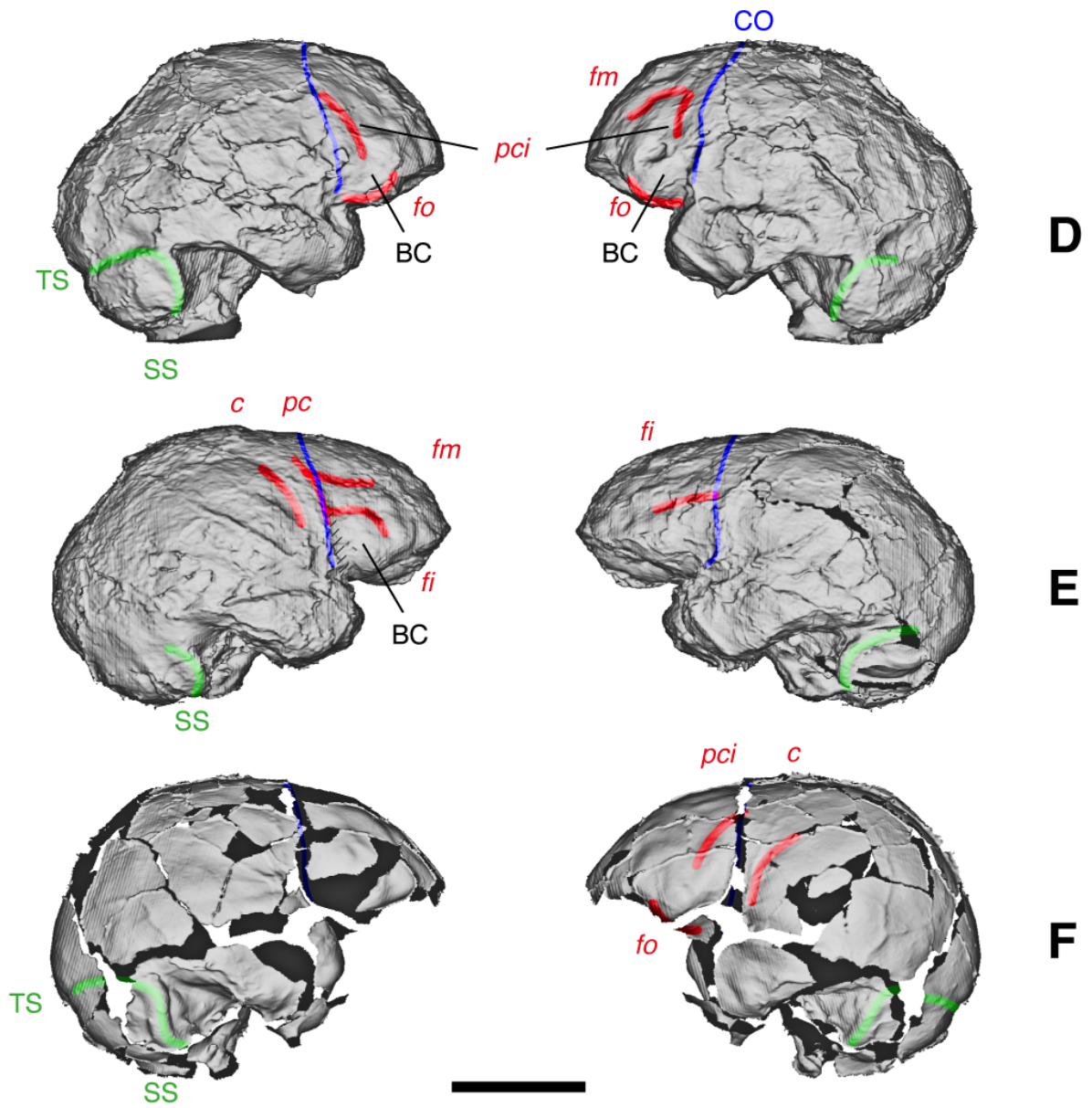


**Fig. S2 D-F.** Endocranial structures of African early *Homo* fossils. **(D)** KNM-ER 3733; **(E)** KNM-ER 3883; **(F)** KNM-WT 15000. Colors and labels as in fig. S1. Hatched area in **(E)**: imprints representing raised margin (lipping) of frontal bone. Scale bar is 5 cm. In KNM-ER 3733 **(D)**, possible imprints of *pci* are situated anterior to CO. In KNM-ER 3883 **(E)**, an imprint attributed to *pc* crosses CO, such that *pci* coincides with, or is slightly anterior to CO. The highly fragmented endocast of KNM-WT 15000 **(F)** shows an imprint of *pci* anterior to CO, and ending superior to BC.

5  
10

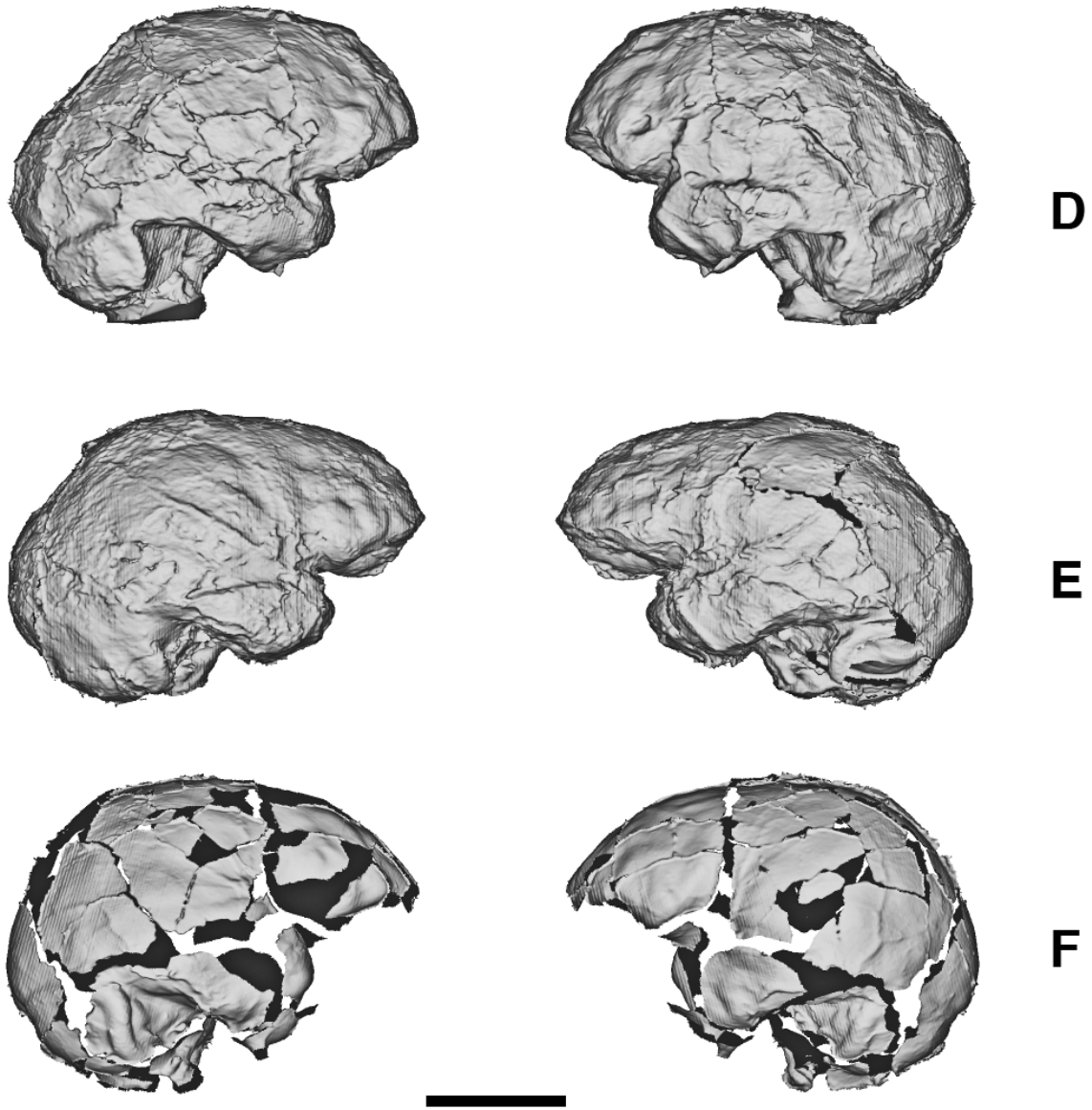


**Fig. S2 D-F.** Endocranial structures of African early *Homo* fossils. **(D)** KNM-ER 3733; **(E)** KNM-ER 3883; **(F)** KNM-WT 15000. Unlabeled 3D reconstructions. Scale bar is 5cm.

5

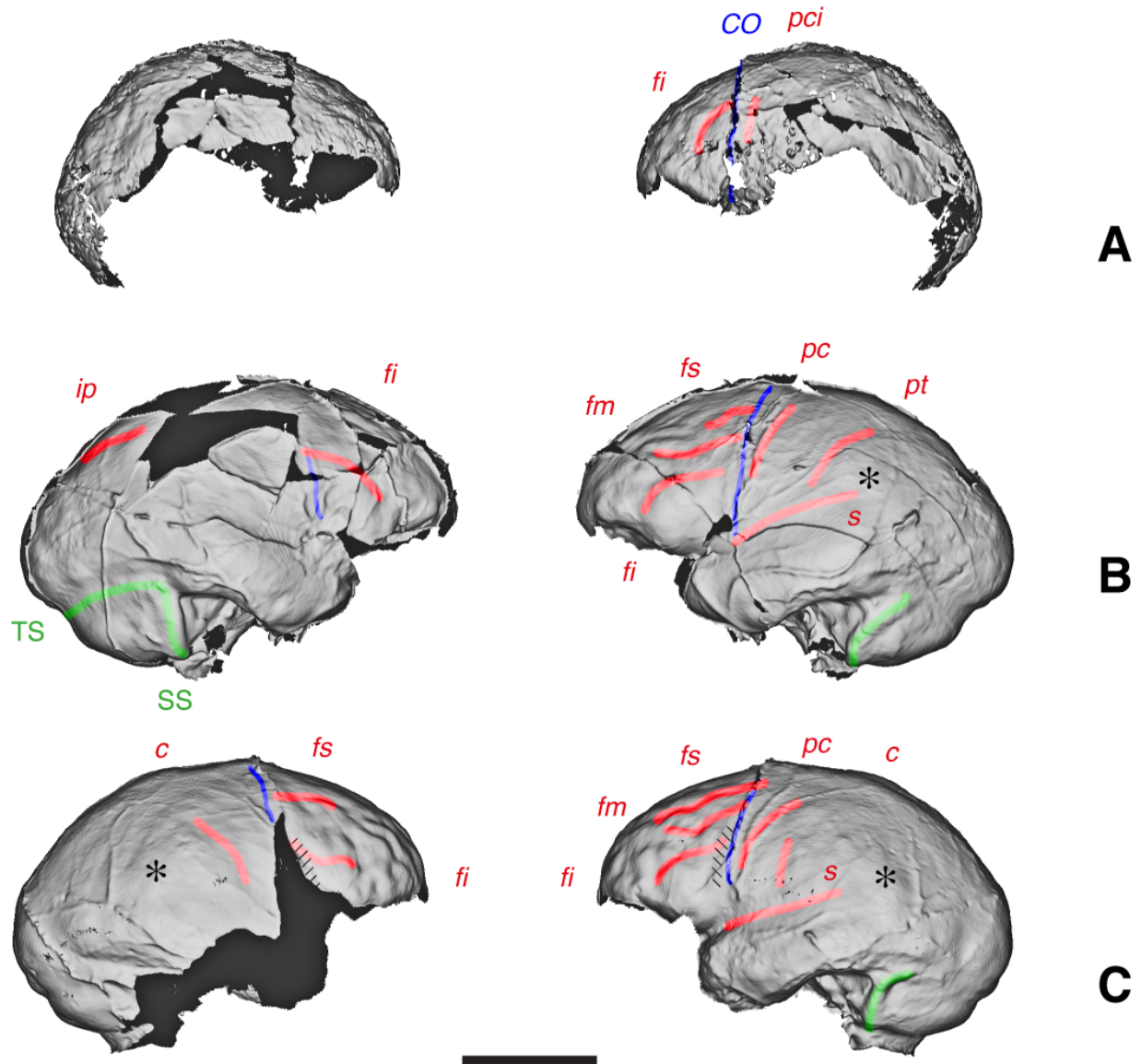


**Fig. S3 A-C.** Endocranial structures of East Asian *Homo erectus* fossils. (A) Mojokerto; (B) Sangiran 17; (C) Bukuran. Colors and labels as in fig. S1. Hatched areas: imprints representing raised bone margins (lipping) of frontal bone; \* symbol: endocranial bulge corresponding to supramarginal gyrus. Scale bar is 5 cm. In all specimens, imprints of the inferior and/or middle frontal sulci (*fi/fm*) terminate at or close to the coronal suture (CO). If visible, imprints of the precentral sulcus (*pc*) are located posterior to CO.

5

10

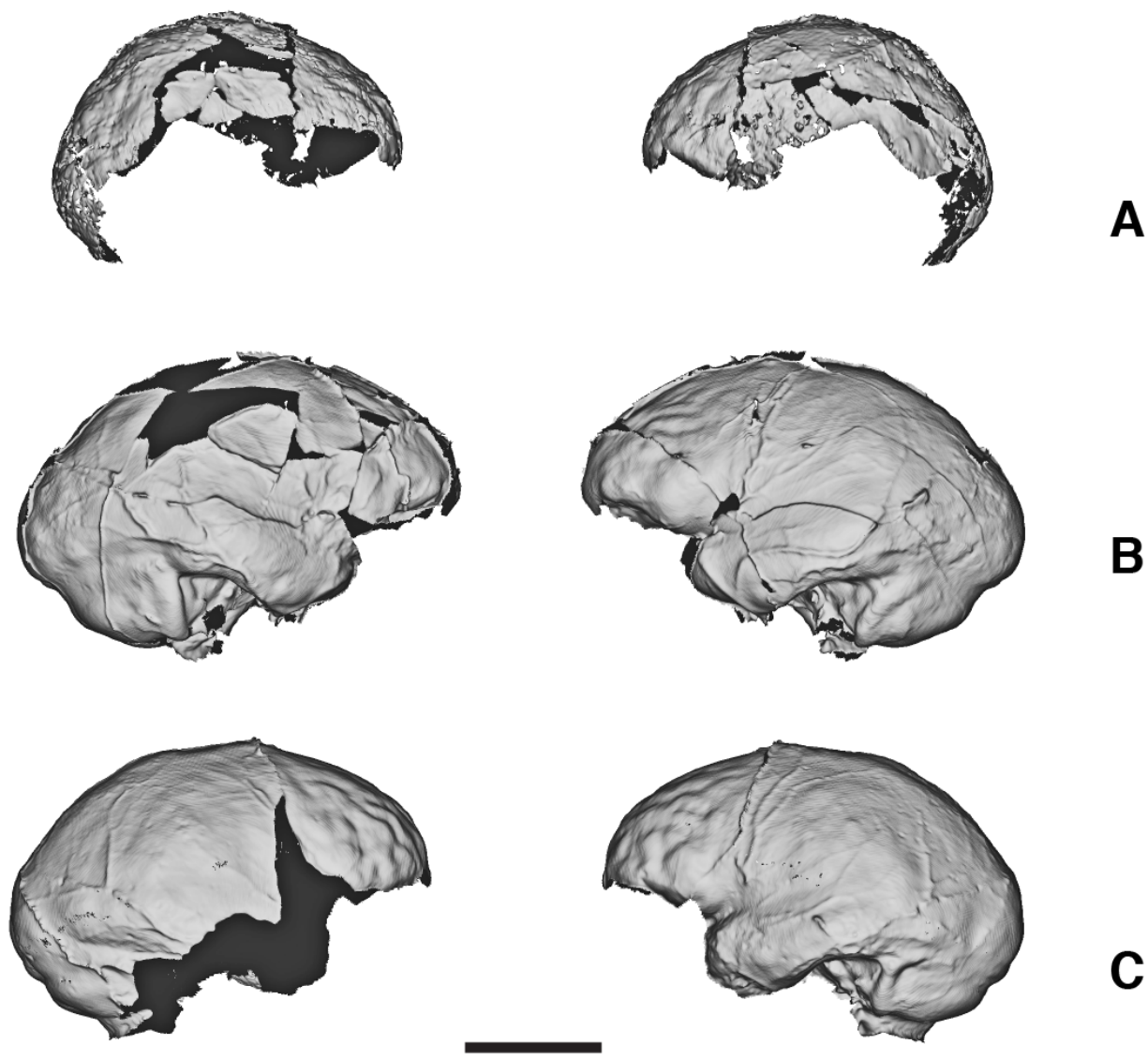


**Fig. S3 A-C.** Endocranial structures of East Asian *Homo erectus* fossils. (A) Mojokerto; (B) Sangiran 17; (C) Bukuran. Unlabeled 3D reconstructions. Scale bar is 5cm.

5

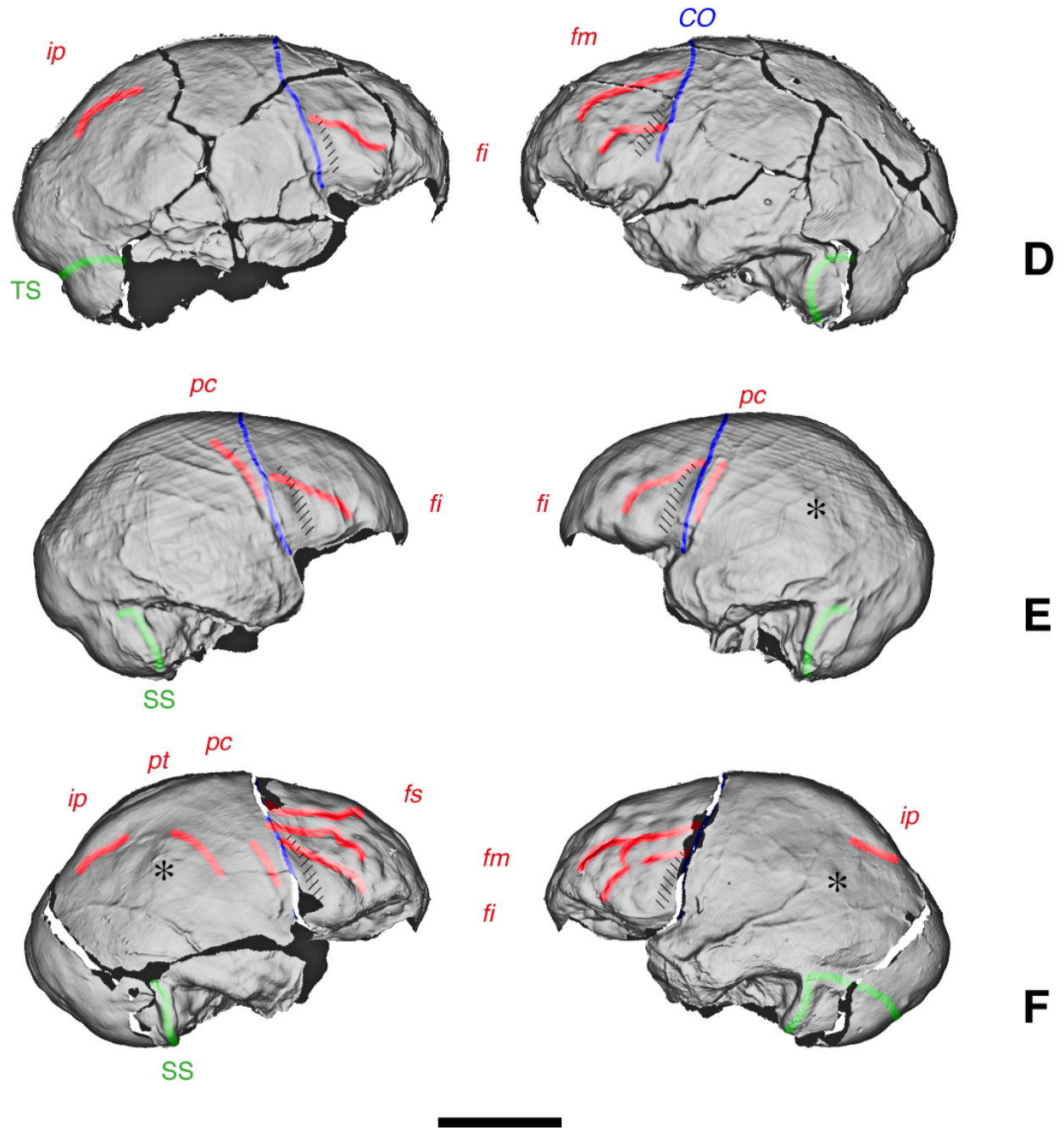
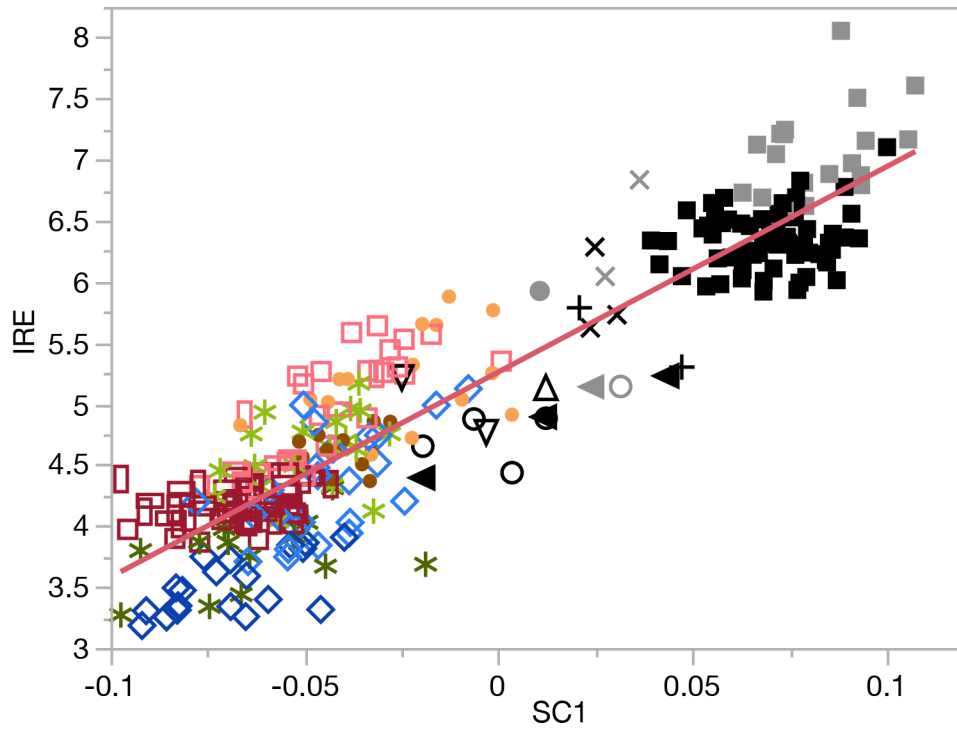


**Fig. S3 D-F.** Endocranial structures of East Asian *Homo erectus* fossils. **(D)** Solo V; **(E)** Sambungmacan 3; **(F)** Zhoukoudian XII. Colors and labels as in fig. S1. Hatched areas: imprints representing raised bone margins (lipping) of frontal bone; \* symbol: endocranial bulge corresponding to supramarginal gyrus. Scale bar is 5 cm. In all specimens, imprints of the inferior and/or middle frontal sulci (*fi/fm*) terminate at or close to the coronal suture (CO). If visible, imprints of the precentral sulcus (*pc*) are located posterior to CO.

5



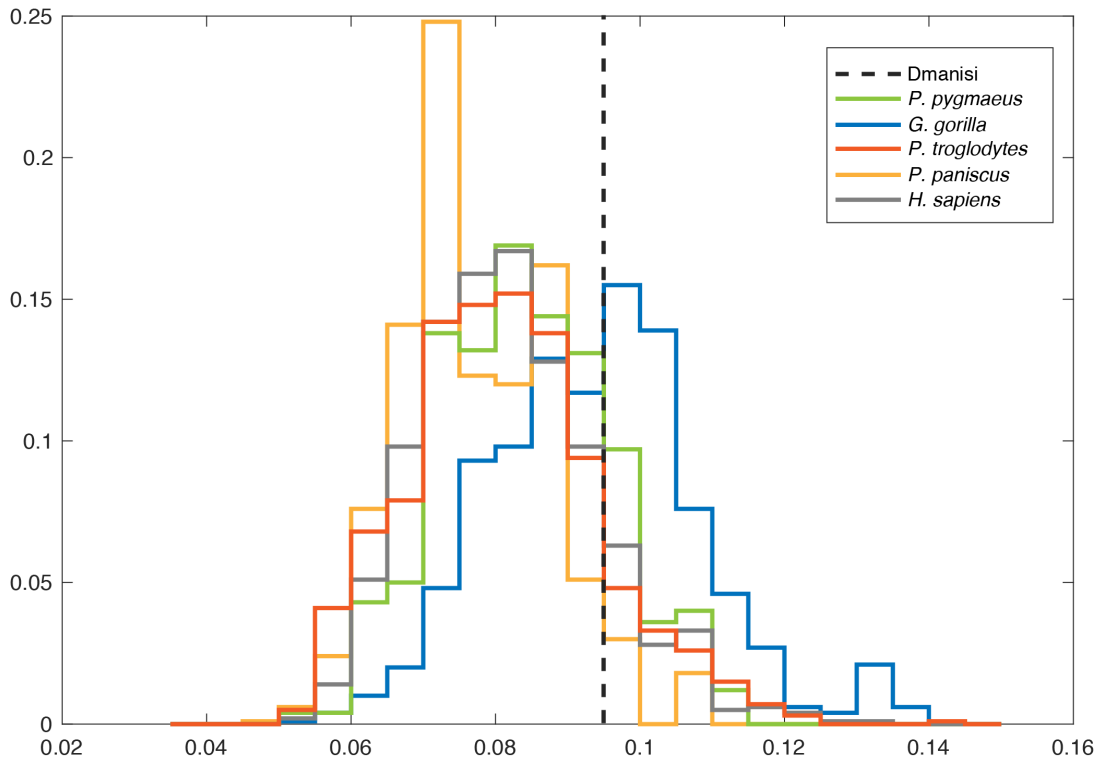
5 **Fig. S3 D-F.** Endocranial structures of East Asian *Homo erectus* fossils. **(D)** Solo V; **(E)** Sambungmacan 3; **(F)** Zhoukoudian XII. Unlabeled 3D reconstructions. Scale bar is 5cm.



5

**Fig. S4.** Regression of IRE [index of relative encephalization, ratio between endocranial size and the size of the face and cranial base; see ref. (38)] against shape component SC1;  $IRE = 5.26 + 16.81 * SC1$ ;  $R^2 = 0.86$ . Symbols see main Fig. 3.

10



5 **Fig. S5.** Ranges of endocranial shape variation in *P. troglodytes*, *P. paniscus*, *G. gorilla*, *P.*  
 10 *pygmaeus*, modern humans (global sample) and in the Dmanisi sample. Dashed line indicates  
 maximum endocranial shape distance between any two specimens in the Dmanisi sample  
 (D2280, D2700, D3444, and D4500); the maximum distance is that between D3444 and D4500.  
 The histograms show species-specific frequency distributions of the maximum endocranial shape  
 distance between any two specimens in random subsamples of  $N=4$  specimens ( $K=1000$   
 resamplings). Note that the maximum shape distance for Dmanisi is well within the species-  
 specific maximum-distance frequency distributions.



## References and Notes

1. C. C. Sherwood, F. Subiaul, T. W. Zawidzki, A natural history of the human mind: Tracing evolutionary changes in brain and cognition. *J. Anat.* **212**, 426–454 (2008). [doi:10.1111/j.1469-7580.2008.00868.x](https://doi.org/10.1111/j.1469-7580.2008.00868.x) [Medline](#)
2. D. Stout, T. Chaminade, Stone tools, language and the brain in human evolution. *Phil. Trans. R. Soc. London Ser. B* **367**, 75–87 (2012). [doi:10.1098/rstb.2011.0099](https://doi.org/10.1098/rstb.2011.0099) [Medline](#)
3. R. L. Holloway, C. C. Sherwood, P. R. Hof, J. K. Rilling, in *Encyclopedia of Neuroscience* (Springer, 2009), pp. 1326–1334.
4. D. Falk, in *Evolution of the Primate Brain: From Neuron to Behavior*, vol. 195 of *Progress in Brain Research*, M. Hofman, D. Falk, Eds. (Elsevier, 2012), pp. 255–272.
5. J. Dumoncel, G. Subsol, S. Durrleman, A. Bertrand, E. de Jager, A. C. Oettlé, Z. Lockhat, F. E. Suleman, A. Beaudet, Are endocasts reliable proxies for brains? A 3D quantitative comparison of the extant human brain and endocast. *J. Anat.* **238**, 480–488 (2021). [doi:10.1111/joa.13318](https://doi.org/10.1111/joa.13318) [Medline](#)
6. A. Balzeau, E. Gilissen, R. L. Holloway, S. Prima, D. Grimaud-Hervé, Variations in size, shape and asymmetries of the third frontal convolution in hominids: Paleoneurological implications for hominin evolution and the origin of language. *J. Hum. Evol.* **76**, 116–128 (2014). [doi:10.1016/j.jhevol.2014.06.006](https://doi.org/10.1016/j.jhevol.2014.06.006) [Medline](#)
7. D. Falk, Interpreting sulci on hominin endocasts: Old hypotheses and new findings. *Front. Hum. Neurosci.* **8**, 134 (2014). [doi:10.3389/fnhum.2014.00134](https://doi.org/10.3389/fnhum.2014.00134) [Medline](#)
8. D. Falk, The evolution of Broca's Area. *IBRO Hist. Neurosci.* **2007**, 2513–2518 (2007).
9. R. L. Holloway, S. D. Hurst, H. M. Garvin, P. T. Schoenemann, W. B. Vanti, L. R. Berger, J. Hawks, Endocast morphology of *Homo naledi* from the Dinaledi Chamber, South Africa. *Proc. Natl. Acad. Sci. U.S.A.* **115**, 5738–5743 (2018). [doi:10.1073/pnas.1720842115](https://doi.org/10.1073/pnas.1720842115) [Medline](#)
10. K. J. Carlson, D. Stout, T. Jashashvili, D. J. de Ruiter, P. Tafforeau, K. Carlson, L. R. Berger, The endocast of MH1, *Australopithecus sediba*. *Science* **333**, 1402–1407 (2011). [doi:10.1126/science.1203922](https://doi.org/10.1126/science.1203922) [Medline](#)
11. D. Falk, C. P. E. Zollikofer, N. Morimoto, M. S. Ponce de León, Metopic suture of Taung (*Australopithecus africanus*) and its implications for hominin brain evolution. *Proc. Natl. Acad. Sci. U.S.A.* **109**, 8467–8470 (2012). [doi:10.1073/pnas.1119752109](https://doi.org/10.1073/pnas.1119752109) [Medline](#)
12. R. L. Holloway, D. C. Broadfield, K. J. Carlson, New high-resolution computed tomography data of the Taung partial cranium and endocast and their bearing on metopism and hominin brain evolution. *Proc. Natl. Acad. Sci. U.S.A.* **111**, 13022–13027 (2014). [doi:10.1073/pnas.1402905111](https://doi.org/10.1073/pnas.1402905111) [Medline](#)
13. D. Falk, C. P. E. Zollikofer, M. Ponce de León, K. Semendeferi, J. L. Alatorre Warren, W. D. Hopkins, Identification of in vivo sulci on the external surface of eight adult chimpanzee brains: Implications for interpreting early hominin endocasts. *Brain Behav. Evol.* **91**, 45–58 (2018). [doi:10.1159/000487248](https://doi.org/10.1159/000487248) [Medline](#)

14. J. S. Allen, J. Bruss, H. Damasio, Looking for the lunate sulcus: A magnetic resonance imaging study in modern humans. *Anat. Rec. A Discov. Mol. Cell. Evol. Biol.* **288**, 867–876 (2006). [doi:10.1002/ar.a.20362](https://doi.org/10.1002/ar.a.20362) [Medline](#)
15. A. A. de Sousa, C. C. Sherwood, H. Mohlberg, K. Amunts, A. Schleicher, C. E. MacLeod, P. R. Hof, H. Frahm, K. Zilles, Hominoid visual brain structure volumes and the position of the lunate sulcus. *J. Hum. Evol.* **58**, 281–292 (2010). [doi:10.1016/j.jhevol.2009.11.011](https://doi.org/10.1016/j.jhevol.2009.11.011) [Medline](#)
16. W. E. LeGros Clark, D. M. Cooper, S. Zuckerman, The endocranial cast of the chimpanzee. *J. R. Anthropol. Inst. G* **66**, 249–268 (1936).
17. C. J. Connolly, *External Morphology of the Primate Brain* (C. C. Thomas, 1950).
18. R. A. Dart, *Australopithecus africanus*: The man-ape of South Africa. *Nature* **115**, 195–199 (1925). [doi:10.1038/115195a0](https://doi.org/10.1038/115195a0)
19. A. Beaudet, R. J. Clarke, E. J. de Jager, L. Bruxelles, K. J. Carlson, R. Crompton, F. de Beer, J. Dhaene, J. L. Heaton, K. Jakata, T. Jashashvili, K. Kuman, J. McClymont, T. R. Pickering, D. Stratford, The endocast of StW 573 (“Little Foot”) and hominin brain evolution. *J. Hum. Evol.* **126**, 112–123 (2019). [doi:10.1016/j.jhevol.2018.11.009](https://doi.org/10.1016/j.jhevol.2018.11.009) [Medline](#)
20. P. Gunz, S. Neubauer, D. Falk, P. Tafforeau, A. Le Cabec, T. M. Smith, W. H. Kimbel, F. Spoor, Z. Alemseged, *Australopithecus afarensis* endocasts suggest ape-like brain organization and prolonged brain growth. *Sci. Adv.* **6**, eaaz4729 (2020). [doi:10.1126/sciadv.aaz4729](https://doi.org/10.1126/sciadv.aaz4729) [Medline](#)
21. D. Falk, Cerebral cortices of East African early hominids. *Science* **221**, 1072–1074 (1983). [doi:10.1126/science.221.4615.1072](https://doi.org/10.1126/science.221.4615.1072) [Medline](#)
22. P. V. Tobias, The brain of *Homo habilis*: A new level of organization in cerebral evolution. *J. Hum. Evol.* **16**, 741–761 (1987). [doi:10.1016/0047-2484\(87\)90022-4](https://doi.org/10.1016/0047-2484(87)90022-4)
23. A. N. Parks, J. B. Smaers, in *Digital Endocasts*, E. Bruner, N. Ogiwara, H. Tanabe, Eds. (Springer, 2018), pp. 205–218.
24. B. Villmoare, W. H. Kimbel, C. Seyoum, C. J. Campisano, E. N. DiMaggio, J. Rowan, D. R. Braun, J. R. Arrowsmith, K. E. Reed, Paleoanthropology. Early Homo at 2.8 Ma from Ledi-Geraru, Afar, Ethiopia. *Science* **347**, 1352–1355 (2015). [doi:10.1126/science.aal1343](https://doi.org/10.1126/science.aal1343) [Medline](#)
25. Y. Rizal, K. E. Westaway, Y. Zaim, G. D. van den Bergh, E. A. Bettis III, M. J. Morwood, O. F. Huffman, R. Grün, R. Joannes-Boyau, R. M. Bailey, M. C. Sidarto, M. C. Westaway, I. Kurniawan, M. W. Moore, M. Storey, F. Aziz, J. Suminto, J. X. Zhao, M. E. Aswan, M. E. Sipola, R. Larick, J. P. Zonneveld, R. Scott, S. Putt, R. L. Ciochon, Last appearance of *Homo erectus* at Ngandong, Java, 117,000–108,000 years ago. *Nature* **577**, 381–385 (2020). [doi:10.1038/s41586-019-1863-2](https://doi.org/10.1038/s41586-019-1863-2) [Medline](#)
26. S. Matsu’ura, M. Kondo, T. Danhara, S. Sakata, H. Iwano, T. Hirata, I. Kurniawan, E. Setiyabudi, Y. Takeshita, M. Hyodo, I. Kitaba, M. Sudo, Y. Danhara, F. Aziz, Age control of the first appearance datum for Javanese *Homo erectus* in the Sangiran area. *Science* **367**, 210–214 (2020). [doi:10.1126/science.aau8556](https://doi.org/10.1126/science.aau8556) [Medline](#)

27. L. Gabunia, A. Vekua, D. Lordkipanidze, C. C. Swisher III, R. Ferring, A. Justus, M. Nioradze, M. Tvalchrelidze, S. C. Antón, G. Bosinski, O. Jöris, M. A. Lumley, G. Majsuradze, A. Mouskhelishvili, Earliest Pleistocene hominid cranial remains from Dmanisi, Republic of Georgia: Taxonomy, geological setting, and age. *Science* **288**, 1019–1025 (2000). [doi:10.1126/science.288.5468.1019](https://doi.org/10.1126/science.288.5468.1019) [Medline](#)
28. R. Ferring, O. Oms, J. Agustí, F. Berna, M. Nioradze, T. Shelia, M. Tappen, A. Vekua, D. Zhvania, D. Lordkipanidze, Earliest human occupations at Dmanisi (Georgian Caucasus) dated to 1.85-1.78 Ma. *Proc. Natl. Acad. Sci. U.S.A.* **108**, 10432–10436 (2011). [doi:10.1073/pnas.1106638108](https://doi.org/10.1073/pnas.1106638108) [Medline](#)
29. A. Vekua, D. Lordkipanidze, G. P. Rightmire, J. Agusti, R. Ferring, G. Maisuradze, A. Mouskhelishvili, M. Nioradze, M. Ponce de León, M. Tappen, M. Tvalchrelidze, C. Zollikofer, A new skull of early *Homo* from Dmanisi, Georgia. *Science* **297**, 85–89 (2002). [doi:10.1126/science.1072953](https://doi.org/10.1126/science.1072953) [Medline](#)
30. D. Lordkipanidze, A. Vekua, R. Ferring, G. P. Rightmire, J. Agusti, G. Kiladze, A. Mouskhelishvili, M. Nioradze, M. S. Ponce de León, M. Tappen, C. P. E. Zollikofer, Anthropology: The earliest toothless hominin skull. *Nature* **434**, 717–718 (2005). [doi:10.1038/434717b](https://doi.org/10.1038/434717b) [Medline](#)
31. D. Lordkipanidze, A. Vekua, R. Ferring, G. P. Rightmire, C. P. E. Zollikofer, M. S. Ponce de León, J. Agusti, G. Kiladze, A. Mouskhelishvili, M. Nioradze, M. Tappen, A fourth hominin skull from Dmanisi, Georgia. *Anat. Rec. A Discov. Mol. Cell. Evol. Biol.* **288**, 1146–1157 (2006). [doi:10.1002/ar.a.20379](https://doi.org/10.1002/ar.a.20379) [Medline](#)
32. D. Lordkipanidze, M. S. Ponce de León, A. Margvelashvili, Y. Rak, G. P. Rightmire, A. Vekua, C. P. E. Zollikofer, A complete skull from Dmanisi, Georgia, and the evolutionary biology of early *Homo*. *Science* **342**, 326–331 (2013). [doi:10.1126/science.1238484](https://doi.org/10.1126/science.1238484) [Medline](#)
33. See supplementary materials.
34. C. P. E. Zollikofer, M. S. Ponce de León, Pandora’s growing box: Inferring the evolution and development of hominin brains from endocasts. *Evol. Anthropol.* **22**, 20–33 (2013). [doi:10.1002/evan.21333](https://doi.org/10.1002/evan.21333) [Medline](#)
35. J. L. Alatorre Warren, M. S. Ponce de León, W. D. Hopkins, C. P. E. Zollikofer, Evidence for independent brain and neurocranial reorganization during hominin evolution. *Proc. Natl. Acad. Sci. U.S.A.* **116**, 22115–22121 (2019). [doi:10.1073/pnas.1905071116](https://doi.org/10.1073/pnas.1905071116) [Medline](#)
36. D. E. Lieberman, C. F. Ross, M. J. Ravosa, The primate cranial base: Ontogeny, function, and integration. *Yearb. Phys. Anthropol.* **43** (suppl. 31), 117–169 (2000). [doi:10.1002/1096-8644\(2000\)43:31+<117:AID-AJPA5>3.0.CO;2-I](https://doi.org/10.1002/1096-8644(2000)43:31+<117:AID-AJPA5>3.0.CO;2-I) [Medline](#)
37. D. E. Lieberman, R. C. McCarthy, The ontogeny of cranial base angulation in humans and chimpanzees and its implications for reconstructing pharyngeal dimensions. *J. Hum. Evol.* **36**, 487–517 (1999). [doi:10.1006/jhev.1998.0287](https://doi.org/10.1006/jhev.1998.0287) [Medline](#)
38. C. P. E. Zollikofer, T. Bienvenu, M. S. Ponce de León, Effects of cranial integration on hominid endocranial shape. *J. Anat.* **230**, 85–105 (2017). [doi:10.1111/joa.12531](https://doi.org/10.1111/joa.12531) [Medline](#)

39. R. L. Holloway, in *Handbook of Paleoanthropology*, W. Henke, I. Tattersall, Eds. (Springer, 2015), vol. 3, pp. 1961–1987.
40. J. K. Rilling, M. F. Glasser, T. M. Preuss, X. Ma, T. Zhao, X. Hu, T. E. J. Behrens, The evolution of the arcuate fasciculus revealed with comparative DTI. *Nat. Neurosci.* **11**, 426–428 (2008). [doi:10.1038/nn2072](https://doi.org/10.1038/nn2072) [Medline](#)
41. J. B. Smaers, D. R. Vanier, Brain size expansion in primates and humans is explained by a selective modular expansion of the cortico-cerebellar system. *Cortex* **118**, 292–305 (2019). [doi:10.1016/j.cortex.2019.04.023](https://doi.org/10.1016/j.cortex.2019.04.023) [Medline](#)
42. O. Bar-Yosef, A. Belfer-Cohen, From Africa to Eurasia—early dispersals. *Quat. Int.* **75**, 19–28 (2001). [doi:10.1016/S1040-6182\(00\)00074-4](https://doi.org/10.1016/S1040-6182(00)00074-4)
43. S. C. Antón, C. C. Swisher III, Early dispersals of *Homo* from Africa. *Annu. Rev. Anthropol.* **33**, 271–296 (2004). [doi:10.1146/annurev.anthro.33.070203.144024](https://doi.org/10.1146/annurev.anthro.33.070203.144024)
44. R. Dennell, W. Roebroeks, An Asian perspective on early human dispersal from Africa. *Nature* **438**, 1099–1104 (2005). [doi:10.1038/nature04259](https://doi.org/10.1038/nature04259) [Medline](#)
45. Y. Kaifu, Archaic hominin populations in Asia before the arrival of modern humans their phylogeny and implications for the “Southern Denisovans”. *Curr. Anthropol.* **58** (S17), S418–S433 (2017). [doi:10.1086/694318](https://doi.org/10.1086/694318)
46. Z. Zhu, R. Dennell, W. Huang, Y. Wu, S. Qiu, S. Yang, Z. Rao, Y. Hou, J. Xie, J. Han, T. Ouyang, Hominin occupation of the Chinese Loess Plateau since about 2.1 million years ago. *Nature* **559**, 608–612 (2018). [doi:10.1038/s41586-018-0299-4](https://doi.org/10.1038/s41586-018-0299-4) [Medline](#)
47. S. S. Putt, S. Wijekumar, R. G. Franciscus, J. P. Spencer, The functional brain networks that underlie Early Stone Age tool manufacture. *Nat. Hum. Behav.* **1**, 0102 (2017). [doi:10.1038/s41562-017-0102](https://doi.org/10.1038/s41562-017-0102)
48. S. S. J. Putt, S. Wijekumar, J. P. Spencer, Prefrontal cortex activation supports the emergence of early stone age toolmaking skill. *Neuroimage* **199**, 57–69 (2019). [doi:10.1016/j.neuroimage.2019.05.056](https://doi.org/10.1016/j.neuroimage.2019.05.056) [Medline](#)
49. C. J. Lepre, H. Roche, D. V. Kent, S. Harmand, R. L. Quinn, J.-P. Brugal, P.-J. Texier, A. Lenoble, C. S. Feibel, An earlier origin for the Acheulian. *Nature* **477**, 82–85 (2011). [doi:10.1038/nature10372](https://doi.org/10.1038/nature10372) [Medline](#)
50. Y. Beyene, S. Katoh, G. Woldegabriel, W. K. Hart, K. Uto, M. Sudo, M. Kondo, M. Hyodo, P. R. Renne, G. Suwa, B. Asfaw, The characteristics and chronology of the earliest Acheulean at Konso, Ethiopia. *Proc. Natl. Acad. Sci. U.S.A.* **110**, 1584–1591 (2013). [doi:10.1073/pnas.1221285110](https://doi.org/10.1073/pnas.1221285110) [Medline](#)
51. S. Semaw, M. J. Rogers, S. W. Simpson, N. E. Levin, J. Quade, N. Dunbar, W. C. McIntosh, I. Cáceres, G. E. Stinchcomb, R. L. Holloway, F. H. Brown, R. F. Butler, D. Stout, M. Everett, Co-occurrence of Acheulian and Oldowan artifacts with *Homo erectus* cranial fossils from Gona, Afar, Ethiopia. *Sci. Adv.* **6**, eaaw4694 (2020). [doi:10.1126/sciadv.aaw4694](https://doi.org/10.1126/sciadv.aaw4694) [Medline](#)
52. M. González-Forero, A. Gardner, Inference of ecological and social drivers of human brain-size evolution. *Nature* **557**, 554–557 (2018). [doi:10.1038/s41586-018-0127-x](https://doi.org/10.1038/s41586-018-0127-x) [Medline](#)

53. K. Teffer, K. Semendeferi, Human prefrontal cortex: Evolution, development, and pathology. *Prog. Brain Res.* **195**, 191–218 (2012). [doi:10.1016/B978-0-444-53860-4.00009-X](https://doi.org/10.1016/B978-0-444-53860-4.00009-X) [Medline](#)
54. B. Dubreuil, C. S. Henshilwood, Archeology and the language-ready brain. *Lang. Cogn.* **5**, 251–260 (2014). [doi:10.1515/langcog-2013-0018](https://doi.org/10.1515/langcog-2013-0018)
55. F. Spoor, M. G. Leakey, P. N. Gathogo, F. H. Brown, S. C. Antón, I. McDougall, C. Kiarie, F. K. Manthi, L. N. Leakey, Implications of new early *Homo* fossils from Ileret, east of Lake Turkana, Kenya. *Nature* **448**, 688–691 (2007). [doi:10.1038/nature05986](https://doi.org/10.1038/nature05986) [Medline](#)
56. F. Spoor, P. Gunz, S. Neubauer, S. Stelzer, N. Scott, A. Kwekason, M. C. Dean, Reconstructed *Homo habilis* type OH 7 suggests deep-rooted species diversity in early *Homo*. *Nature* **519**, 83–86 (2015). [doi:10.1038/nature14224](https://doi.org/10.1038/nature14224) [Medline](#)
57. M. G. Leakey, F. Spoor, M. C. Dean, C. S. Feibel, S. C. Antón, C. Kiarie, L. N. Leakey, New fossils from Koobi Fora in northern Kenya confirm taxonomic diversity in early *Homo*. *Nature* **488**, 201–204 (2012). [doi:10.1038/nature11322](https://doi.org/10.1038/nature11322) [Medline](#)
58. I. McDougall, F. H. Brown, P. M. Vasconcelos, B. E. Cohen, D. S. Thiede, M. J. Buchanan, New single crystal <sup>40</sup>Ar/<sup>39</sup>Ar ages improve time scale for deposition of the Omo Group, Omo-Turkana Basin, East Africa. *J. Geol. Soc. London* **169**, 213–226 (2012). [doi:10.1144/0016-76492010-188](https://doi.org/10.1144/0016-76492010-188)
59. P. N. Gathogo, F. H. Brown, Revised stratigraphy of Area 123, Koobi Fora, Kenya, and new age estimates of its fossil mammals, including hominins. *J. Hum. Evol.* **51**, 471–479 (2006). [doi:10.1016/j.jhevol.2006.05.005](https://doi.org/10.1016/j.jhevol.2006.05.005) [Medline](#)
60. A. Walker, R. Leakey, *The Nariokotome Homo erectus Skeleton* (Springer, 1993).
61. L. J. McHenry, I. G. Stanistreet, Tephrochronology of Bed II, Olduvai Gorge, Tanzania, and placement of the Oldowan-Acheulean transition. *J. Hum. Evol.* **120**, 7–18 (2018). [doi:10.1016/j.jhevol.2017.12.006](https://doi.org/10.1016/j.jhevol.2017.12.006) [Medline](#)
62. S. Neubauer, P. Gunz, L. Leakey, M. Leakey, J.-J. Hublin, F. Spoor, Reconstruction, endocranial form and taxonomic affinity of the early *Homo calvaria* KNM-ER 42700. *J. Hum. Evol.* **121**, 25–39 (2018). [doi:10.1016/j.jhevol.2018.04.005](https://doi.org/10.1016/j.jhevol.2018.04.005) [Medline](#)
63. W. H. Gilbert, B. Asfaw, *Homo erectus: Pleistocene Evidence from the Middle Awash, Ethiopia* (Univ. California Press, 2009), vol. 1.
64. E. Bruner, L. Bondioli, A. Coppa, D. W. Frayer, R. L. Holloway, Y. Libsekal, T. Medin, L. Rook, R. Macchiarelli, The endocast of the one-million-year-old human cranium from Buia (UA 31), Danakil Eritrea. *Am. J. Phys. Anthropol.* **160**, 458–468 (2016). [doi:10.1002/ajpa.22983](https://doi.org/10.1002/ajpa.22983) [Medline](#)
65. G. C. Conroy, G. W. Weber, H. Seidler, W. Recheis, D. Zur Nedden, J. H. Mariam, Endocranial capacity of the bodo cranium determined from three-dimensional computed tomography. *Am. J. Phys. Anthropol.* **113**, 111–118 (2000). [doi:10.1002/1096-8644\(200009\)113:1<111:AID-AJPA10>3.0.CO;2-X](https://doi.org/10.1002/1096-8644(200009)113:1<111:AID-AJPA10>3.0.CO;2-X) [Medline](#)
66. R. Grün, A. Pike, F. McDermott, S. Eggins, G. Mortimer, M. Aubert, L. Kinsley, R. Joannes-Boyau, M. Rumsey, C. Denys, J. Brink, T. Clark, C. Stringer, Dating the skull from

- Broken Hill, Zambia, and its position in human evolution. *Nature* **580**, 372–375 (2020). [doi:10.1038/s41586-020-2165-4](https://doi.org/10.1038/s41586-020-2165-4) [Medline](#)
67. D. Grimaud-Hervé, D. Lordkipanidze, in *Paleoneurological Studies in Honor of Ralph L. Holloway*, D. Broadfield, M. Yuan, K. Schick, N. Toth, Eds. (Stone Age Institute Press, 2010), pp. 59–82.
68. F. Weidenreich, Some particulars of skull and brain of early hominids and their bearing on the problem of the relationship between man and anthropoids. *Am. J. Phys. Anthropol.* **5**, 387–428 (1947). [doi:10.1002/ajpa.1330050402](https://doi.org/10.1002/ajpa.1330050402) [Medline](#)
69. X. Wu, L. A. Schepartz, D. Falk, W. Liu, Endocranial cast of Hexian *Homo erectus* from South China. *Am. J. Phys. Anthropol.* **130**, 445–454 (2006). [doi:10.1002/ajpa.20378](https://doi.org/10.1002/ajpa.20378) [Medline](#)
70. F. Tilney, H. A. Riley, *The Brain from Ape to Man* (P. B. Hoeber, 1928).
71. J. C. A. Joordens, F. d’Errico, F. P. Wesselingh, S. Munro, J. de Vos, J. Wallinga, C. Ankjærgaard, T. Reimann, J. R. Wijbrans, K. F. Kuiper, H. J. Mûcher, H. Coqueugniot, V. Prié, I. Joosten, B. van Os, A. S. Schulp, M. Panuel, V. van der Haas, W. Lustenhouwer, J. J. G. Reijmer, W. Roebroeks, *Homo erectus* at Trinil on Java used shells for tool production and engraving. *Nature* **518**, 228–231 (2015). [doi:10.1038/nature13962](https://doi.org/10.1038/nature13962) [Medline](#)
72. X. J. Wu, L. A. Schepartz, C. J. Norton, Morphological and morphometric analysis of variation in the Zhoukoudian *Homo erectus* brain endocasts. *Quat. Int.* **211**, 4–13 (2010). [doi:10.1016/j.quaint.2009.07.002](https://doi.org/10.1016/j.quaint.2009.07.002)
73. J. Ash, G. G. Gallup Jr., Paleoclimatic variation and brain expansion during human evolution. *Hum. Nat.* **18**, 109–124 (2007). [doi:10.1007/s12110-007-9015-z](https://doi.org/10.1007/s12110-007-9015-z) [Medline](#)
74. Y. Kaifu, Y. Zaim, H. Baba, I. Kurniawan, D. Kubo, Y. Rizal, J. Arif, F. Aziz, New reconstruction and morphological description of a *Homo erectus* cranium: Skull IX (Tjg-1993.05) from Sangiran, Central Java. *J. Hum. Evol.* **61**, 270–294 (2011). [doi:10.1016/j.jhevol.2011.04.002](https://doi.org/10.1016/j.jhevol.2011.04.002) [Medline](#)
75. H. Baba, F. Aziz, S. Narasaki, Restoration of head and face in Javanese *Homo erectus* Sangiran 17. *Bull Natl. Sci. Mus. Tokyo* **24**, 1–8 (1998).
76. E. Indriati, S. C. Antón, The calvaria of Sangiran 38, Sendangbusik, Sangiran Dome, Java. *Homo* **61**, 225–243 (2010). [doi:10.1016/j.jchb.2010.05.002](https://doi.org/10.1016/j.jchb.2010.05.002) [Medline](#)
77. D. Grimaud-Hervé, H. Widiyanto, F. Détroit, F. Sémah, Comparative morphological and morphometric description of the hominin calvaria from Bukuran (Sangiran, Central Java, Indonesia). *J. Hum. Evol.* **63**, 637–652 (2012). [doi:10.1016/j.jhevol.2012.07.001](https://doi.org/10.1016/j.jhevol.2012.07.001) [Medline](#)
78. A. Balzeau, D. Grimaud-Hervé, T. Jacob, Internal cranial features of the Mojokerto child fossil (East Java, Indonesia). *J. Hum. Evol.* **48**, 535–553 (2005). [doi:10.1016/j.jhevol.2005.01.002](https://doi.org/10.1016/j.jhevol.2005.01.002) [Medline](#)
79. M. J. Morwood, P. O’Sullivan, E. Susanto, F. Aziz, Revised age for Mojokerto 1, an early *Homo erectus* cranium from East Java, Indonesia. *Aust. Archaeol.* **57**, 1–4 (2003). [doi:10.1080/03122417.2003.11681757](https://doi.org/10.1080/03122417.2003.11681757)

80. D. C. Broadfield, R. L. Holloway, K. Mowbray, A. Silvers, M. S. Yuan, S. Márquez, Endocast of Sambungmacan 3 (Sm 3): A new *Homo erectus* from Indonesia. *Anat. Rec.* **262**, 369–379 (2001). [doi:10.1002/ar.1047](https://doi.org/10.1002/ar.1047) [Medline](#)
81. H. Baba, F. Aziz, Y. Kaifu, G. Suwa, R. T. Kono, T. Jacob, *Homo erectus* calvarium from the Pleistocene of Java. *Science* **299**, 1384–1388 (2003). [doi:10.1126/science.1081676](https://doi.org/10.1126/science.1081676) [Medline](#)
82. Y. Kaifu, I. Kurniawan, D. Kubo, E. Sudiyabudi, G. P. Putro, E. Prasanti, F. Aziz, H. Baba, *Homo erectus* calvaria from Ngawi (Java) and its evolutionary implications. *Anthropol. Sci.* **123**, 161–176 (2015). [doi:10.1537/ase.150702](https://doi.org/10.1537/ase.150702)
83. R. L. Holloway, Indonesian “Solo” (Ngandong) endocranial reconstructions: Some preliminary observations and comparisons with Neandertal and *Homo erectus* groups. *Am. J. Phys. Anthropol.* **53**, 285–295 (1980). [doi:10.1002/ajpa.1330530213](https://doi.org/10.1002/ajpa.1330530213) [Medline](#)
84. P. Brown, T. Sutikna, M. J. Morwood, R. P. Soejono, E. Jatmiko, E. W. Saptomo, R. A. Due, A new small-bodied hominin from the Late Pleistocene of Flores, Indonesia. *Nature* **431**, 1055–1061 (2004). [doi:10.1038/nature02999](https://doi.org/10.1038/nature02999) [Medline](#)
85. D. Kubo, R. T. Kono, Y. Kaifu, Brain size of *Homo floresiensis* and its evolutionary implications. *Proc. Biol. Sci.* **280**, 20130338 (2013). [doi:10.1098/rspb.2013.0338](https://doi.org/10.1098/rspb.2013.0338) [Medline](#)
86. T. Sutikna, M. W. Tocheri, M. J. Morwood, E. W. Saptomo, R. D. Jatmiko, R. D. Awe, S. Wasisto, K. E. Westaway, M. Aubert, B. Li, J. X. Zhao, M. Storey, B. V. Alloway, M. W. Morley, H. J. Meijer, G. D. van den Bergh, R. Grün, A. Dosseto, A. Brumm, W. L. Jungers, R. G. Roberts, Revised stratigraphy and chronology for *Homo floresiensis* at Liang Bua in Indonesia. *Nature* **532**, 366–369 (2016). [doi:10.1038/nature17179](https://doi.org/10.1038/nature17179) [Medline](#)
87. T. Bienvenu, F. Guy, W. Coudyzer, E. Gilissen, G. Roualdès, P. Vignaud, M. Brunet, Assessing endocranial variations in great apes and humans using 3D data from virtual endocasts. *Am. J. Phys. Anthropol.* **145**, 231–246 (2011). [doi:10.1002/ajpa.21488](https://doi.org/10.1002/ajpa.21488) [Medline](#)
88. S. S. Keller, M. Deppe, M. Herbin, E. Gilissen, Variability and asymmetry of the sulcal contours defining Broca’s area homologue in the chimpanzee brain. *J. Comp. Neurol.* **520**, 1165–1180 (2012). [doi:10.1002/cne.22747](https://doi.org/10.1002/cne.22747) [Medline](#)
89. G. J. Jenkins, Cranio-cerebral topography. *J. Anat. Physiol.* **39**, 462–470 (1905). [Medline](#)
90. Y. Kobayashi, T. Matsui, N. Ogihara, in *Digital Endocasts*, E. Bruner, N. Ogihara, H. Tanabe, Eds. (Springer, 2018), pp. 33–46.
91. G. Ribas, *Applied Cranial-Cerebral Anatomy: Brain Architecture and Anatomically Oriented Microneurosurgery* (Cambridge Univ. Press, 2018).
92. F. L. Bookstein, in *Image Fusion and Shape Variability Techniques* (Leeds Univ. Press, 1996), pp. 59–70.
93. S. Schlager, Morpho: Calculations and visualisations related to Geometric Morphometrics (2014); <https://sourceforge.net/projects/morpho-rpackage>.

94. D. C. Adams, E. Otarola-Castillo, geomorph: An R package for the collection and analysis of geometric morphometric shape data. *Methods Ecol. Evol.* **4**, 393–399 (2013). [doi:10.1111/2041-210X.12035](https://doi.org/10.1111/2041-210X.12035)
95. C. P. E. Zollikofer, M. S. Ponce de León, Visualizing patterns of craniofacial shape variation in *Homo sapiens*. *Proc. Biol. Sci.* **269**, 801–807 (2002). [doi:10.1098/rspb.2002.1960](https://doi.org/10.1098/rspb.2002.1960) [Medline](#)
96. A. Balzeau, E. Gilissen, D. Grimaud-Hervé, Shared pattern of endocranial shape asymmetries among great apes, anatomically modern humans, and fossil hominins. *PLOS ONE* **7**, e29581 (2011). [doi:10.1371/journal.pone.0029581](https://doi.org/10.1371/journal.pone.0029581) [Medline](#)
97. S. Neubauer, P. Gunz, N. A. Scott, J. J. Hublin, P. Mitteroecker, Evolution of brain lateralization: A shared hominid pattern of endocranial asymmetry is much more variable in humans than in great apes. *Sci. Adv.* **6**, eaax9935 (2020). [doi:10.1126/sciadv.aax9935](https://doi.org/10.1126/sciadv.aax9935) [Medline](#)
98. F. Tilney, The brain of prehistoric man. *Arch. Neurol. Psychiatry* **17**, 723–769 (1927). [doi:10.1001/archneurpsyc.1927.02200360003001](https://doi.org/10.1001/archneurpsyc.1927.02200360003001)
99. F. Weidenreich, Observations on the form and proportions of the endocranial casts of *Sinanthropus pekinensis*, other hominids and the Great Apes: A comparative study of brain size. *Palaeontol. Sin. Ser. D* **7**, 1–50 (1936).
100. C. Kappers, K. Bouman, Comparison of the endocranial casts of the *Pithecanthropus erectus* skull found by Dubois and von Koenigswald's *Pithecanthropus* skull. *Proc. R. Acad. Amsterdam* **42**, 1–12 (1939).
101. R. L. Holloway, The Indonesian *Homo erectus* brain endocasts revisited. *Am. J. Phys. Anthropol.* **55**, 503–521 (1981). [doi:10.1002/ajpa.1330550412](https://doi.org/10.1002/ajpa.1330550412)
102. R. L. Holloway, D. Broadfield, M. Yuan, *Brain Endocasts – The Paleoneurological Evidence*, vol. 3 of *The Human Fossil Record*, G. T. Schwartz, I. Tattersall, Eds. (Wiley, 2004).
103. F. Weidenreich, *Morphology of Solo Man* (Anthropological Papers of the American Museum of Natural History, vol. 43, part 3, New York, 1951).
104. O. Huffman, J. De Vos, A. Berkhout, F. Aziz, Provenience reassessment of the 1931–1933 Ngandong *Homo erectus* (Java), confirmation of the bone-bed origin reported by the discoverers. *Paleoanthropology* **2010**, 1–60 (2010). [doi:10.4207/PA.2010.ART34](https://doi.org/10.4207/PA.2010.ART34)
105. R. Pickering, P. H. G. M. Dirks, Z. Jinnah, D. J. de Ruiter, S. E. Churchil, A. I. R. Herries, J. D. Woodhead, J. C. Hellstrom, L. R. Berger, *Australopithecus sediba* at 1.977 Ma and implications for the origins of the genus *Homo*. *Science* **333**, 1421–1423 (2011). [doi:10.1126/science.1203697](https://doi.org/10.1126/science.1203697) [Medline](#)
106. P. H. G. M. Dirks, E. M. Roberts, H. Hilbert-Wolf, J. D. Kramers, J. Hawks, A. Dosseto, M. Duval, M. Elliott, M. Evans, R. Grün, J. Hellstrom, A. I. R. Herries, R. Joannes-Boyau, T. V. Makhubela, C. J. Placzek, J. Robbins, C. Spandler, J. Wiersma, J. Woodhead, L. R. Berger, The age of *Homo naledi* and associated sediments in the Rising Star Cave, South Africa. *eLife* **6**, e24231 (2017). [doi:10.7554/eLife.24231](https://doi.org/10.7554/eLife.24231) [Medline](#)



107. D. Falk, C. Hildebolt, K. Smith, M. J. Morwood, T. Sutikna, P. Brown, Jatmiko, E. W. Saptomo, B. Brunnsden, F. Prior, The brain of LB1, *Homo floresiensis*. *Science* **308**, 242–245 (2005). [doi:10.1126/science.1109727](https://doi.org/10.1126/science.1109727) [Medline](#)